nature structural & molecular biology

Article

https://doi.org/10.1038/s41594-025-01502-y

Haspin kinase binds to a nucleosomal DNA supergroove

Received: 19 May 2024

Accepted: 29 January 2025

Published online: 20 February 2025

Check for updates

Chad W. Hicks[1], Colin R. Gliech[2], Sanim Rahman[1], Xiangbin Zhang[1], Andrew S. Eneim[1], Stacy J. Vasquez[1], Andrew J. Holland[2] & Cynthia Wolberger[1]

Phosphorylation of histone H3 threonine 3 (H3T3) by Haspin recruits the chromosomal passenger complex to the inner centromere and ensures proper cell cycle progression through mitosis. The mechanism by which Haspin binds to nucleosomes to phosphorylate H3T3 is not known. Here we report cryogenic electron microscopy structures of the human Haspin kinase domain bound to a nucleosome. In contrast with previous structures of histone-modifying enzymes, Haspin solely contacts the nucleosomal DNA, inserting into a supergroove formed by apposing major grooves of two DNA gyres. This binding mode provides a plausible mechanism by which Haspin can bind to nucleosomes in a condensed chromatin environment to phosphorylate H3T3. We identify key basic residues in the Haspin kinase domain that are essential for phosphorylation of nucleosomal histone H3 and binding to mitotic chromatin. Our structural data provide notable insight into a histone-modifying enzyme that binds to nucleosomes solely through DNA contacts.

Post-translational modification of histones regulates fundamental biological processes, including transcription, DNA replication, the DNA damage response and the cell cycle[1]. Histone phosphorylation regulates the cell cycle by triggering a cascade of histone modifications to promote chromatin condensation during mitosis[2,3]. Phosphorylation of histone H3 threonine 3 (H3T3ph) and histone H2A threonine 120 (H2AT120ph), two of the most prominent mitotic phosphoryl modifications[4], define the centromere–kinetochore region. H3T3ph localizes to the inner centromere while H2AT120ph localizes to the kinetochore-proximal outer centromere[5]. H3T3ph is established at the nuclear envelope in early prophase, becomes most concentrated during metaphase and gradually diminishes during anaphase[6]. The Repo-Man/PP1γ complex dephosphorylates H3T3ph to oppose the spread of this modification to chromosome arms in early mitosis and catalyzes the removal of H3T3ph at the end of mitosis[7]. H3T3ph recruits the chromosomal passenger complex (CPC) to the inner centromere[4,8,9], while H2AT120ph primarily recruits the CPC to the kinetochore-proximal outer centromere[5]. The CPC, one of the main controllers of mitosis[10], contains the highly conserved Aurora B kinase, which phosphorylates multiple histone H3 residues[11] and many kinetochore proteins[12] in the centromere–kinetochore region.

The Haspin kinase establishes and maintains wild-type levels of H3T3ph during mitosis[13,14] and is conserved in most eukaryotes, including yeast, plants, flies and worms[15,16]. The only known substrate of Haspin is histone H3T3. Depletion or inhibition of Haspin abolishes H3T3ph[14], displaces the CPC from inner centromeres[17], causes premature chromatid separation[18], prevents normal chromosome alignment[14] and delays mitotic progression[17,19]. The BUB1 kinase can partially compensate for loss of Haspin by phosphorylating histone H2A-T120 in the kinetochore-proximal outer centromere[5], which also partially contributes to CPC recruitment at the inner centromere[5,20–22]. Although earlier studies have argued that the H3T3 kinase, VRK1, is also important for generating H3T3ph during mitosis[23,24], more recent work suggests that VRK1 is not essential for generating mitotic H3T3ph, while Haspin is essential[25]. Because Haspin is important for ensuring proper mitotic progression[13,14] and is overexpressed in many cancers[26], there have been extensive efforts to identify and characterize compounds that inhibit Haspin H3T3 phosphorylation activity[27–31].

[1]Department of Biophysics and Biophysical Chemistry, Johns Hopkins University School of Medicine, Baltimore, MD, USA. [2]Department of Molecular Biology and Genetics, Johns Hopkins University School of Medicine, Baltimore, MD, USA. e-mail: cwolberg@jhmi.edu

Human Haspin is a 798-amino-acid protein that contains a ~450 residue disordered N-terminal region and a C-terminal atypical kinase domain[27,32–34]. Haspin's structured C-terminal kinase domain has a bilobal shape similar to that of proteins belonging to the eukaryotic protein kinase family[15,27,34], one of the largest families of eukaryotic proteins[35]. Haspin contains a negatively charged active-site cleft between its two structured lobes where the histone H3 tail and adenosine triphosphate (ATP), the phosphate donor, bind[27,36]. Mono-, di- and trimethylation of histone H3 lysine 4 (H3K4me1/2/3), which is commonly found at actively transcribed genes[37], inhibit Haspin activity[27], probably through steric clash of the methylated lysine within the enzyme's acidic active-site cleft[36]. Haspin is regulated by a basic region (residues 383–394) within the disordered N-terminus, which auto-inhibits Haspin kinase activity[38]. The AlphaFold-predicted structure[39] of full-length Haspin suggests that this basic region partially occludes the Haspin active site (AlphaFold-Q8TF76-F1). Phosphorylation of multiple Haspin N-terminal residues by Cdk1 and Plk1 activates Haspin[38,40], probably by releasing the basic N-terminal segment from the active site. The N-terminus also plays an important role in recruiting Haspin to centromeric chromatin by interacting with the Pds5 subunit of the cohesin complex[41].

Whereas the structural basis by which Haspin recognizes the histone H3 tail is well characterized[27,34,36], nothing is known about how this enzyme engages an intact nucleosome substrate. While many chromatin-binding proteins contact the nucleosome acidic patch and other residues in the histone octamer core[42–44], these surfaces are often occluded in a condensed chromatin environment. It is not known how Haspin binds to nucleosomes in these conditions.

We report here the structure of the Haspin kinase domain bound to a nucleosome determined by cryogenic electron microscopy (cryo-EM). Unlike all previously reported structures of nucleosome binding proteins, Haspin does not contact the globular histone core. Instead, Haspin exclusively contacts the DNA, inserting into a cavity formed by apposed major grooves of two adjacent gyres of nucleosomal DNA. Haspin engages the unique geometry of this DNA supergroove[45] with basic residues that contact the negatively charged DNA sugar-phosphate backbone. The positioning of Haspin in the supergroove between superhelical locations (SHLs) 5.5 and −2.5 enables Haspin to bind the histone H3 tail and engage its H3T3 substrate. Our structure of a histone kinase domain bound to chromatin reveals an unexpected mode of nucleosome binding that can allow Haspin to phosphorylate its histone substrate in both open and condensed chromatin.

Results

Cryo-EM structure of Haspin bound to a nucleosome

To investigate the structural basis by which Haspin binds nucleosomes, we used cryo-EM to determine structures of the Haspin kinase domain (residues 465–798) bound to nucleosome core particles wrapped with 185 bp of DNA containing the 147 bp Widom 601 sequence flanked by 19 bp linkers (185 bp) (Table 1 and Extended Data Fig. 1). Samples were prepared by mixing Haspin with nucleosome in the absence of crosslinker and flash-freezing on cryo-EM grids (Methods). The cryo-EM density maps revealed Haspin bound to the side of the nucleosome disk, engaging both gyres of nucleosomal DNA (Fig. 1a,b). We identified two similar but distinct orientations of Haspin, denoted positions 1 and 2 (Fig. 1c). The global resolution estimates for the electron microscopy (EM) maps of Haspin in positions 1 and 2 were 3.01 Å and 2.99 Å, respectively (Extended Data Fig. 2a,b). The local resolution of Haspin in position 1 is ~4 Å and ~5 Å in position 2 (Extended Data Fig. 2c,d). Within the EM density for each Haspin kinase domain, the resolution is highest at the interface between Haspin and the nucleosome. The fit for the Haspin model in position 1 was slightly better than for Haspin in position 2, but the secondary structure of both Haspin molecules fits well within their respective EM maps (Extended Data Fig. 2e,f). The structure of the Haspin kinase domain is very similar to previously published crystal structures[27,34,36] (Extended Data Fig. 3), indicating that there are no notable conformational changes in Haspin upon binding to nucleosome.

Table 1 | Cryo-EM data collection, refinement and validation statistics

	Haspin position 1	Haspin position 2	Haspin local refinement
Data collection and processing			
Magnification (×)	130,000	130,000	130,000
Voltage (kV)	300	300	300
Electron exposure (e^{-} Å^{-2})	40	40	40
Dose rate (e^{-} per pixel per second)	7.74	7.74	7.74
Defocus range (μM)	−0.5 to −2.5	−0.5 to −2.5	−0.5 to −2.5
Pixel size (Å)	0.970	0.970	0.970
Camera	Falcon 4	Falcon 4	Falcon 4
Energy filter slit width (eV)	10	10	10
Micrographs	9,362	9,362	9,362
Initial cleaned particle stack	900,411	900,411	900,411
Particle duplication symmetry	–	–	–
Final particles	152,199	154,151	481,127
Map resolution at 0.143 FSC cutoff (Å)	3.01	2.99	3.64
Refinement			
Initial models used (PDB)	Nuc: 4ZUX Haspin: 4OUC	Nuc: 4ZUX Haspin: 4OUC	H3: 4OUC Haspin: 4OUC
Map resolution range (Å)	2.00 to 6.00	2.00 to 6.00	2.00 to 10.00
Model resolution at 0.5 FSC cutoff (Å)	3.2	3.2	4.3
Nonhydrogen atoms	15,497	15,194	2,672
Nucleotides	314	314	0
Ligands	0	0	0
Protein B factor (Å^2)	84.34	116.92	135.69
Nucleotide B factor (Å^2)	102.40	131.09	–
Ligand B factor (Å^2)	–	–	–
Bond length RMSD (Å)	0.005	0.004	0.004
Bond angles RMSD (°)	0.618	0.583	1.081
Validation			
MolProbity score	1.67	1.80	1.97
Clashscore	7.37	7.94	14.78
Rotamer outliers (%)	0.52	2.24	0.67
Ramachandran favored (%)	96.08	97.50	95.74
Ramachandran allowed (%)	3.92	2.50	4.26
Ramachandran disallowed (%)	0.00	0.00	0.00

FSC, Fourier shell correlation; RMSD, root mean square deviation.

https://doi.org/10.1038/s41594-025-01502-y

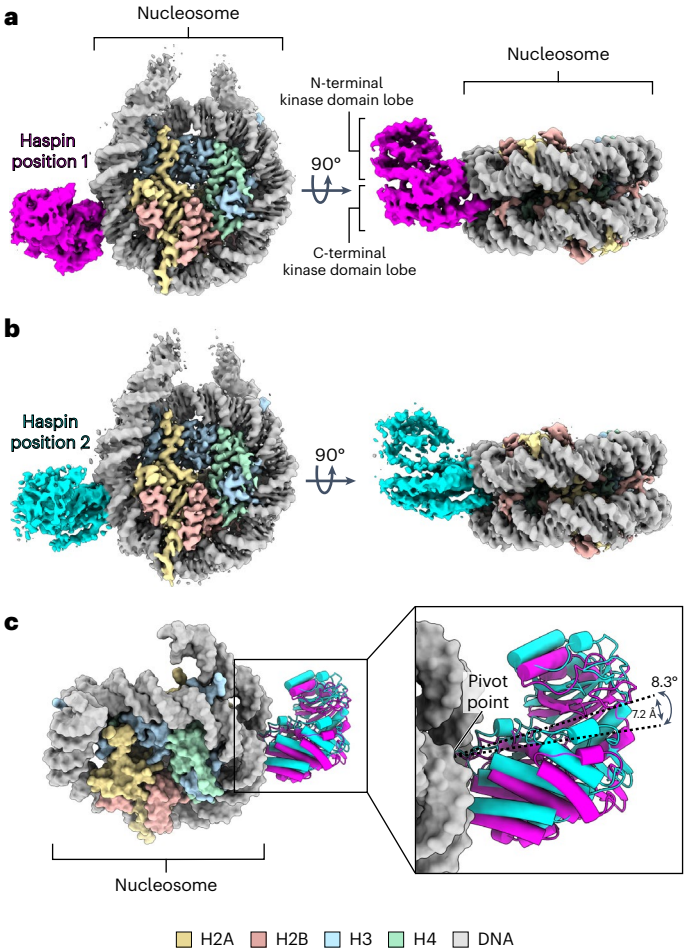

Fig. 1 | Haspin binds to nucleosomal DNA. a, Cryo-EM map of Haspin (465–798) in position 1 bound to nucleosome. **b**, Cryo-EM map of Haspin (465–798) in position 2 bound to nucleosome. **c**, Superposition of the nucleosomes for cryo-EM models of Haspin bound to nucleosome in positions 1 and 2. The Haspin cartoon models show an 8.3° pivot between the two Haspin positions with the pivot point origin located at the SHL 5.5 major groove.

Haspin binds to a nucleosome supergroove

Haspin binds to nucleosomes via a unique DNA-binding mechanism. Unlike all other structures of histone-modifying enzymes bound to nucleosome reported so far[42–44], the Haspin kinase domain does not contact the histone core. Instead, the enzyme binds to nucleosomal DNA by inserting into a large cavity formed by the apposition of major grooves on the two neighboring gyres of nucleosomal DNA, termed a supergroove[45] (Fig. 2a). There are multiple such supergrooves at different locations around the nucleosome core particle. The specific supergroove to which Haspin binds is composed of the major grooves at SHLs 5.5 and −2.5 (Fig. 2a). To the best of our knowledge, a protein binding to a nucleosome in this manner has not been previously observed.

Extensive electrostatic interactions between the positively charged surface of the Haspin kinase domain and the negatively charged DNA stabilize Haspin binding to the nucleosome (Fig. 2b). The positive ends of the Haspin αE and αH helix dipoles insert into the DNA supergroove (Fig. 2c), while residues K759 and K761 in the loop connecting helices αF and αH form electrostatic interactions with the sugar-phosphate backbone on either side of the major groove at SHL 5.5 (Fig. 2c–e). In addition, K659 forms electrostatic interactions with the sugar-phosphate backbone adjacent to SHL 5.5 (Fig. 2c,f), and R772 interacts with the DNA phosphate backbone adjacent to SHL −2.5 (Fig. 2c,g). Side-chain and main-chain atoms of K759 and T760 are sufficiently close to DNA bases at positions 55 and −56 to form van der Waals interactions. We note that the DNA sequence in this location is not identical in the twofold symmetry-related nucleosomal DNA, but the density is ambiguous, suggesting that our maps probably represent an average of particles containing Haspin bound to one or the other symmetry-related supergrooves. There are otherwise no apparent contacts with the DNA bases.

The identification of two distinct Haspin positions on the nucleosome suggests that there is some flexibility in the positioning of Haspin within the supergroove. Superposition of the nucleosomes in the models corresponding to Haspin positions 1 and 2 shows that the kinase domain rotates by ~8.3° about a pivot point located in the DNA major groove at SHL 5.5 (Fig. 1c). The direction of the rotational change in Haspin position follows the curve of the major groove at SHL 5.5. Although Haspin contacts both DNA gyres, the rotational change in enzyme position about a pivot point at SHL 5.5 suggests that interactions with the SHL 5.5 DNA gyre play a more dominant role in positioning Haspin than interactions with the SHL −2.5 DNA gyre.

Binding of the histone H3 tail to Haspin

The end of the H3 tail in the Haspin active site was poorly resolved, probably due to heterogeneity in the position of Haspin bound to nucleosome (Fig. 1c). To better resolve the H3 tail, we removed the EM density corresponding to nucleosome from the cryo-EM particle stack using signal subtraction and performed local refinement and alignment of the Haspin kinase domain alone (Table 1 and Extended Data Fig. 1) to a final resolution of 3.64 Å (Extended Data Fig. 4a). The local resolution

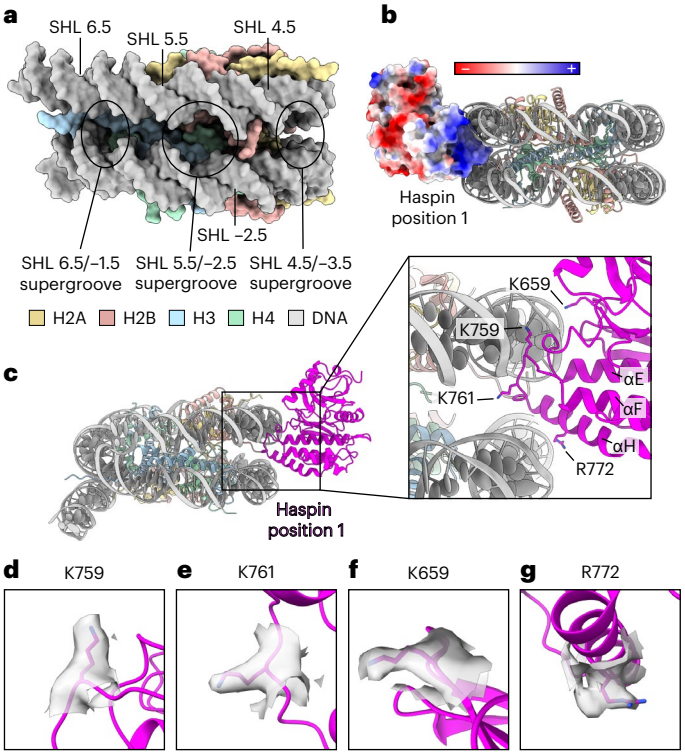

Fig. 2 | Electrostatic interactions stabilize Haspin binding to the nucleosomal DNA supergroove. a, A nucleosome surface representation showing how DNA major grooves on adjacent nucleosomal DNA gyres form nucleosomal DNA supergrooves at different SHLs. The black circles highlight the different nucleosomal DNA supergrooves. **b**, A surface model of Haspin colored in electrostatic representation and bound to nucleosome in position 1. **c**, A cartoon model of Haspin bound to nucleosome in position 1. The inset shows a magnified view of key Haspin residues interacting with nucleosomal DNA. **d**–**g**, Cryo-EM side-chain density for key Haspin residues K759 (**d**), K761 (**e**), K659 (**f**) and R772 (**g**).

https://doi.org/10.1038/s41594-025-01502-y

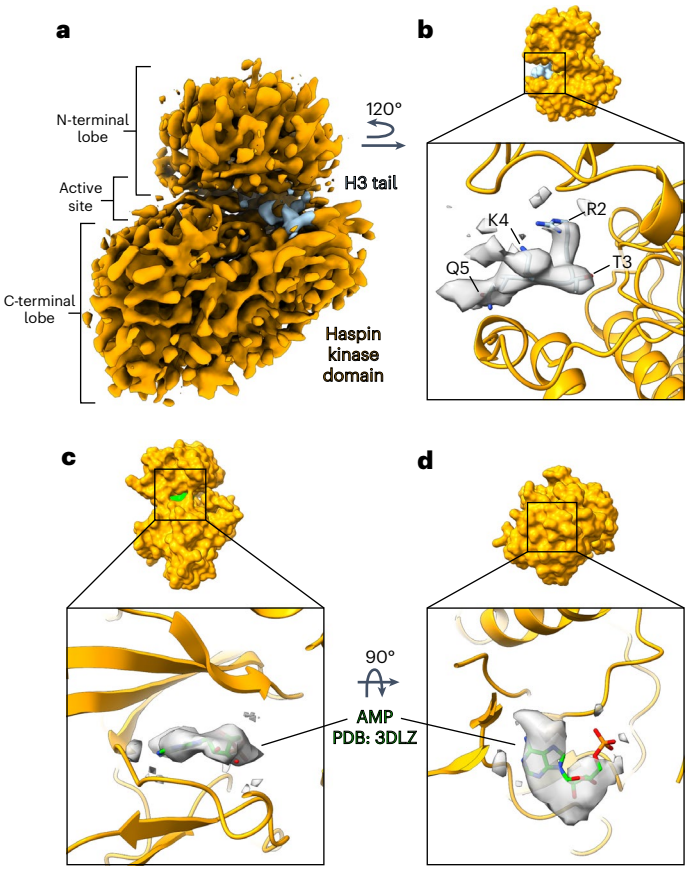

Fig. 3 | Density corresponding the histone H3 tail and a small molecule in the Haspin active site. a, Cryo-EM map of locally refined Haspin (465–798) from a cryo-EM dataset of Haspin-bound nucleosome. **b**, Cryo-EM surface and cartoon models of Haspin (465–798) showing H3 tail bound to the active site with good EM density for H3 tail side chains (2–5). **c**,**d**, Cryo-EM surface and cartoon models of Haspin (465–798) showing density for a small molecule bound to the Haspin ATP cofactor site, in side view (**c**) and top view (**d**). A previously reported Haspin structure (PDB: 3DLZ) with bound AMP molecule was superimposed over our cryo-EM map of Haspin and fits well within our EM density.

of the Haspin local refinement ranged from ~2 Å at the center of the EM map to ~10 Å at the periphery (Extended Data Fig. 4b), allowing a better Haspin model fit at the center of the EM map than at the periphery (Extended Data Fig. 4c). We observed well-resolved EM density for H3 residues 2–5 showing a 180° turn of the H3 tail, positioning H3R2, H3T3 and H3K4 deep within the Haspin acidic cleft (Fig. 3a,b). The structure and contacts formed by these H3 residues are very similar to those observed in a previously determined crystal structure of Haspin bound to H3 tail peptide (residues 1–7) (Protein Data Bank (PDB): 4OUC)[36] (Extended Data Fig. 5a,b).

Although no ATP or nucleotide analogs were added during sample preparation, we also observed density for a small molecule in the Haspin ATP binding site (Fig. 3c,d). We presume that the density corresponds to a small molecule that bound to Haspin during its overexpression and remained bound during purification. Superposition of the crystal structure of Haspin kinase domain bound to adenosine monophosphate (AMP) (PDB: 3DLZ)[27] shows a good fit of an AMP molecule to the EM density (Fig. 3c,d).

While we did not observe strong EM density for residues 5–36 of the histone H3 tail in our initial unsharpened cryo-EM maps (Fig. 1a,b), low-pass filtering the map of Haspin bound to nucleosome in position 1 revealed low-resolution density for the H3 tail (Fig. 4a). The H3 tail follows a path along the nucleosomal DNA, bridging the gap to Haspin's structured N-terminal kinase domain lobe and inserting into the Haspin active site (Fig. 4b). While individual residues cannot be resolved in this map, this portion of the H3 tail contains multiple positively charged residues that could form favorable electrostatic interactions with the negatively charged DNA backbone (Fig. 4c). We note that the model shown represents one of a number of possible fits of the H3 tail to the density. The low resolution of the EM density for the tail indicates that these residues are highly mobile and can adopt multiple conformations along the tail's path to the Haspin active site.

To investigate the role of the H3 tail in Haspin binding to nucleosome, we compared the binding affinity of Haspin on canonical unmodified nucleosomes and on tailless unmodified nucleosomes using electrophoretic mobility shift assays (EMSAs) (Extended Data Fig. 6). Increasing concentrations of Haspin resulted in the formation of a faint shifted band, which presumably corresponds to a 1:1 complex of Haspin bound to nucleosome. At the highest concentrations of Haspin, a high-molecular-weight smear resulting from nonspecific aggregates of Haspin and nucleosome appeared. We qualitatively compared the binding affinity of Haspin on canonical nucleosomes and on tailless nucleosomes by visualizing the disappearance of the free nucleosome band (Extended Data Fig. 6). At a concentration of 1 µM Haspin on canonical nucleosomes, the free nucleosome band had disappeared, indicating that the nucleosome species were completely bound. At the same concentration of Haspin on tailless

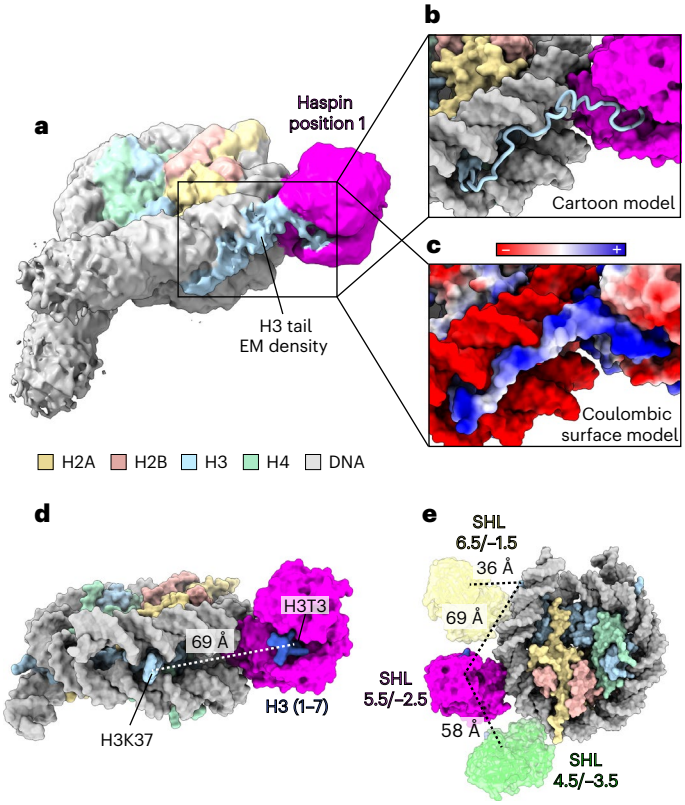

Fig. 4 | Haspin binds in an optimal position for engaging the H3 tail. **a**, Gaussian-filtered cryo-EM map of Haspin bound to nucleosome in position 1 at a very low threshold showing EM density for the H3 tail. **b**, Atomic model of Haspin bound to nucleosome in position 1 depicting a path for the histone H3 tail into the Haspin active site. **c**, Cryo-EM surface model colored in coulombic surface representation. **d**, Superimposition of the cryo-EM model of Haspin in position 1 and the crystal structure of Haspin bound to H3 tail peptide (dark blue) (PDB: 4OUC)[36] showing a 69 Å distance from the H3T3 and the last well-ordered H3 tail residue in the cryo-EM model (residue H3K37) (light blue). **e**, Distance calculations between H3K37 of the cryo-EM structure of Haspin bound to nucleosome and H3T3 of hypothetical Haspin binding positions in the SHL 6.5/−1.5 or SHL 4.5/−3.5 supergroove.

https://doi.org/10.1038/s41594-025-01502-y

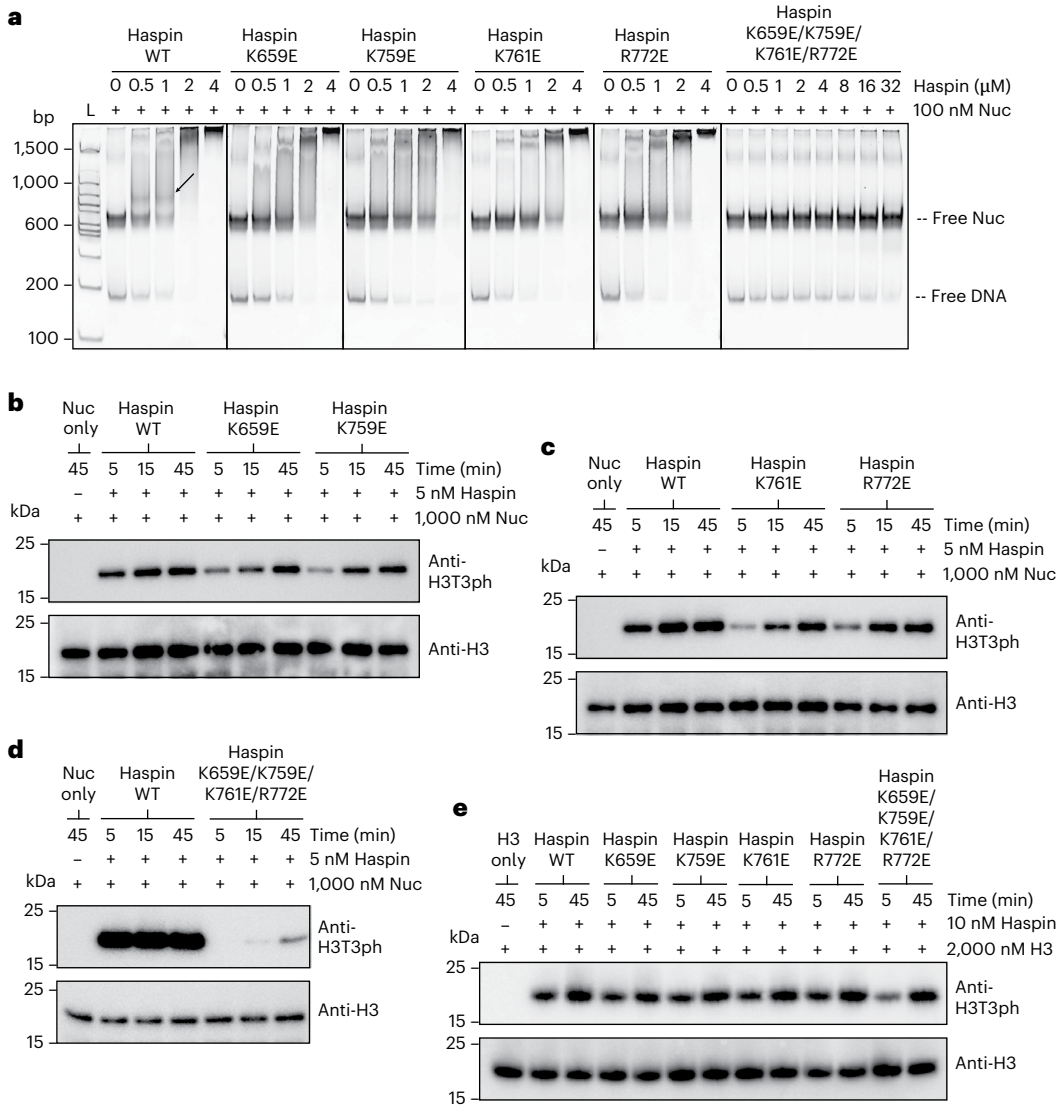

Fig. 5 | Charge-reversal substitution of key Haspin residues disrupts Haspin binding to nucleosome and H3T3 phosphorylation activity. a, EMSAs showing binding of wild-type Haspin (465–798) and Haspin mutants (465–798) to nucleosome (Nuc) at the indicated concentrations. The black arrow points to a band indicative of a Haspin–nucleosome complex. EMSAs corresponding to wild-type Haspin and four-mutant Haspin were performed twice with similar results, while the single-mutant Haspin EMSAs were performed once. **b**–**d**, Immunoblots showing the activity of wild-type Haspin and Haspin mutants K659E and K759E (**b**), K761E and R772E (**c**) and K659E/K759E/K761E/R772E (**d**) on nucleosomes. Experiments on wild-type Haspin and single-mutant Haspin were performed twice with similar results, while the experiment on four-mutant Haspin was performed once. **e**, Immunoblot showing the activity of wild-type Haspin and Haspin mutants on free histone H3. The experiment was performed once. The activity was measured by incubating with an antibody against H3T3ph. Loading controls were run on a separate gel and incubated with an antibody against histone H3.

nucleosomes, the free nucleosome band was greatly diminished but still visible, indicating that the nucleosome species were only partially bound. Therefore, the histone H3 tail partially contributes to Haspin binding to the nucleosome and may affect Haspin positioning on the nucleosome.

The observed positioning of Haspin on the nucleosome optimizes the enzyme's interactions with the tail of histone H3. There are six major supergrooves in the nucleosome core particle, with three on one side related to the other three by the nucleosome dyad symmetry. Binding to the SHL 5.5/−2.5 DNA supergroove places the Haspin active site ~69 Å from H3K37, the last well-ordered histone H3 residue, which emerges between the DNA gyres (Fig. 4d). Because the maximum distance that can be covered by H3 residues 3–37 is ~119 Å, binding to the SHL 5.5/−2.5 DNA supergroove positions Haspin at an optimal distance to bind the extended histone H3 tail with Thr3 in the enzyme active site. In this position, the basic residues in the extended H3 tail can form favorable electrostatic interactions with the negatively charged DNA backbone. Binding to the adjacent major supergroove at SHL 4.5/−3.5 would place the Haspin active site ~127 Å from H3K37 (Fig. 4e), which is probably too far away to bind to H3T3. Although binding to the supergroove at SHL 6.5/−1.5 would place the Haspin active site only ~36 Å from H3K37, well within reach of H3T3 (Fig. 4e), we did not observe EM density for Haspin in this supergroove. We note that the H3 tail would need to form a long loop or fold upon itself to place H3T3 within the enzyme active site at the SHL 6.5/−1.5 supergroove. A less extended conformation of the H3 tail would probably reduce the potential to form ionic interactions with the DNA, making this a less-favored binding site for Haspin. Future experiments are warranted to further elucidate the positional effects of Haspin binding to a specific nucleosomal DNA groove on its phosphorylation activity.

https://doi.org/10.1038/s41594-025-01502-y

Since the 2.5/−5.5 supergroove is symmetrically analogous to the 5.5/−2.5 supergroove, Haspin should be able to bind to both supergrooves, which would result in particles corresponding to 2:1 Haspin:nucleosome complexes. However, our analysis of the cryo-EM data revealed particles with just one Haspin kinase domain bound to a nucleosome, or no bound enzyme at all. We speculate that the harsh conditions of the air–water interface during vitrification disrupted the Haspin–nucleosome interaction such that there were very few remaining 2:1 Haspin–nucleosome complexes and more free nucleosomes than what would be expected in solution at the same concentrations of Haspin and nucleosome. Consistent with this explanation, 47% of nucleosomes in the cryo-EM data were not bound by Haspin (Extended Data Fig. 1) and needed to be removed using three-dimensional (3D) classification to obtain a stack of particles containing only nucleosomes with bound Haspin.

Basic residues are important for Haspin binding and activity

To evaluate the contributions of individual Haspin residues to nucleosome binding, we assayed the effects of point substitutions on the affinity of Haspin for nucleosomes using EMSAs. Increasing concentrations of wild-type Haspin resulted in the formation of a discrete shifted band, which presumably corresponds to a 1:1 complex of Haspin bound to nucleosome (Fig. 5a). At the highest concentrations of Haspin, a high-molecular-weight smear resulting from nonspecific aggregates of Haspin and nucleosome appeared. In binding assays of Haspin point mutants containing the charge-reversal substitutions, K659E, K759E, K761E or R772E, the discrete band corresponding to a complex of Haspin bound to nucleosome is lost (Fig. 5a). Introducing all four substitutions in Haspin abrogated all detectable binding to nucleosomes, even at an enzyme concentration of 32 µM (Fig. 5a).

To confirm the relevance of the observed Haspin–DNA contacts to kinase activity, we assayed the effects of Haspin mutations on the phosphorylation of nucleosomal histone H3T3. Point substitutions K659E, K759E, K761E and R772E in Haspin all reduced the rate of H3T3 phosphorylation as compared with wild-type enzyme (Fig. 5b,c). Incorporating all four charge-reversal substitutions into Haspin dramatically reduced activity (Fig. 5d). These substitutions had very little effect on the ability of Haspin to phosphorylate free histone H3 (Fig. 5e), confirming that the mutations affect nucleosome binding only, not enzymatic activity.

We next tested whether the residues identified as important for DNA binding and activity in vitro are also important for chromatin binding and activity of full-length Haspin in cells. HEK293T cells were transfected with enhanced green fluorescent protein (EGFP)-tagged Haspin to assess its association with mitotic chromosomes. Consistent with previous reports, wild-type EGFP–Haspin colocalized with 4′,6-diamidino-2-phenylindole (DAPI)-stained DNA in fixed cell imaging (Fig. 6a). Strikingly, incorporating all four charge-reversal mutations (K659E, K759E, K761E and R772E) caused a greater than fourfold reduction in the colocalization of Haspin with chromatin as compared with wild-type Haspin and was comparable to the EGFP-only control (Fig. 6b). Interestingly, some cells transfected with the Haspin mutant formed protein aggregates (Fig. 6a), which were not observed in cells transfected with wild-type Haspin. Incorporating all four charge-reversal Haspin mutations also led to a loss of H3T3 phosphorylation and was comparable to the EGFP-only control (Fig. 6c). This result showing a loss of H3T3 phosphorylation in cells using the full-length Haspin mutant is consistent with our result showing a dramatic reduction of H3T3 phosphorylation in vitro using the Haspin kinase domain mutant (Fig. 5d). Taken together, these results support the importance of the DNA contacts observed in the cryo-EM structure of the Haspin kinase domain bound to a nucleosome.

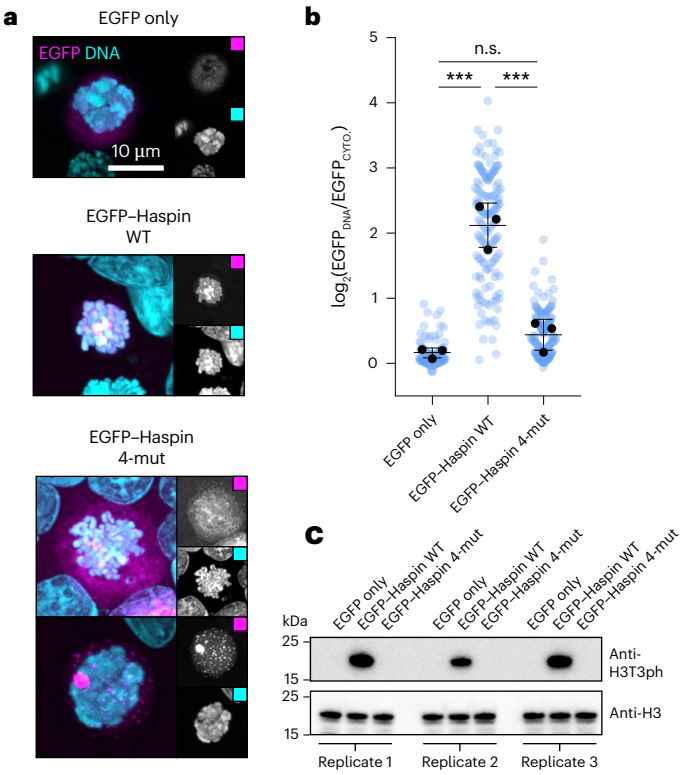

Fig. 6 | Positively charged Haspin kinase domain residues are important for recruiting full-length Haspin to chromatin and promoting H3T3 phosphorylation in cells. a, Fixed-cell fluorescence microscopy of mitotic HEK293T cells transfected with EGFP alone, EGFP–Haspin wild type (WT) and EGFP–Haspin K659E/K759E/K761E/R772E (4-mut). Magenta is EGFP, and cyan is DNA (DAPI stain). **b**, The ratio of cytoplasmic and DNA colocalized median EGFP signal from mitotic images. Images were collected from three independent transfections. The large black dots represent average intensity ratios from each experiment. The blue dots represent intensity ratios for individual images. $N = 3$ independent experiments, $n \geq 25$ cells per condition. Data are represented as mean ± s.d. (for black dots). The data were analyzed using one-way analysis of variance with a post-hoc Tukey's multiple comparisons test on log-transformed values. Adjusted P values: GFP versus GFP–Haspin (WT), 0.0002; GFP versus GFP–Haspin (4-mut), 0.3971; GFP–Haspin (WT) versus GFP–Haspin (4-mut), 0.0004. n.s., not significant. **c**, An immunoblot showing H3T3 phosphorylation activity of EGFP only, EGFP–Haspin WT and EGFP–Haspin 4-mut transfections in HEK293T cells. The experiment was performed once using three biological replicates. The activity was measured by incubating with an antibody against H3T3ph. Loading controls were run on a separate gel and incubated with an antibody against histone H3.

Discussion

Previous investigations had revealed the mechanism by which Haspin engages an H3 tail peptide[36], but it was not known how Haspin recognizes an intact nucleosome substrate. Our structure unexpectedly shows that the Haspin kinase domain binds solely to the nucleosomal DNA, inserting into the cavity called a supergroove[45] that is formed by two adjacent DNA major grooves (Figs. 1 and 2). To the best of our knowledge, a protein that binds to this unique feature of nucleosomes and a structure of a histone-modifying enzyme that does not contact the globular histone octamer core have not been previously reported.

The potential of DNA supergrooves for specific interactions with proteins was first proposed by Edayathumangalam, Luger and colleagues[45] in their study of a polyamide that binds to two adjacent minor grooves in the nucleosome. It was noted that the nucleosome contains multiple major and minor supergrooves, each arising from

https://doi.org/10.1038/s41594-025-01502-y

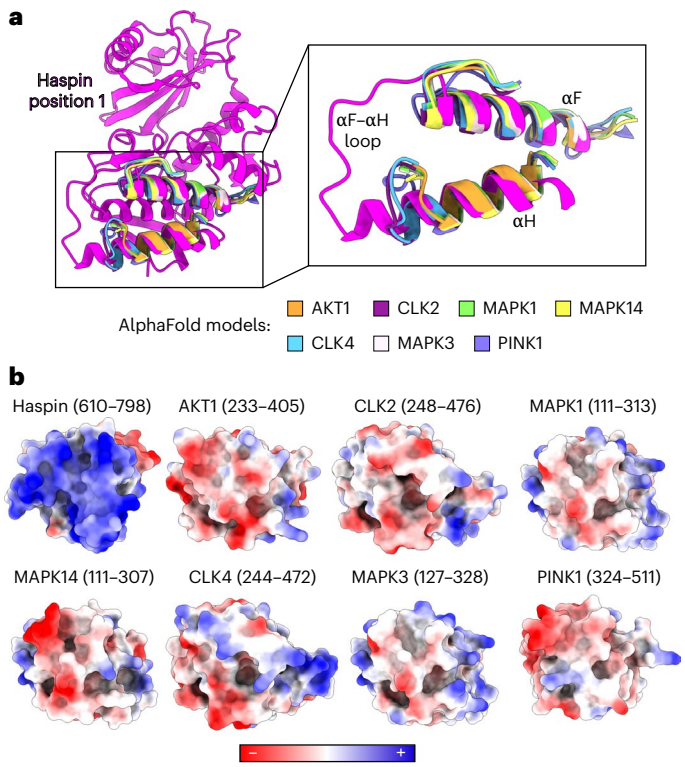

Fig. 7 | Haspin DNA supergroove binding surface is unique among structurally related proteins. a, Foldseek structural homology search using Haspin (610–798) as the search query and superimposition over Haspin. The inset shows Haspin (738–783), AKT1 (327–347, 372–383), CLK2 (358–380, 443–459), MAPK1 (205–227, 281–294), MAPK14 (200–222, 276–289), CLK4 (354–376, 439–456), MAPK3 (223–244, 298–311) and PINK1 (430–452, 476–490) in cartoon model representation. **b**, Superimposition of Haspin and structurally related proteins in coulombic surface representation showing the difference in charge of the Haspin DNA binding surface.

the apposition of DNA major and minor grooves on adjacent DNA gyres. While these supergrooves were proposed as potential sites that could be recognized by proteins that form sequence-specific base-pair contacts within the supergroove[45], Haspin primarily contacts the sugar-phosphate backbone of the DNA and does not appear to recognize specific bases. This lack of specific interactions is consistent with the biological role of Haspin, which must bind to nucleosomes with diverse sequences.

The observed electrostatic interactions between the Haspin kinase domain and nucleosomal DNA are essential for Haspin binding to nucleosomes in vitro (Fig. 5) and to chromatin in cells (Fig. 6a,b). Previous studies had shown that Haspin can bind DNA[32] and speculated that the many positively charged residues in the unstructured N-terminus of Haspin mediated DNA binding[15,32,33]. However, we have shown that charge-reversal substitutions of four key basic residues in the Haspin kinase domain almost completely abolish Haspin localization to mitotic chromatin in HEK293T cells (Fig. 6a,b), thereby preventing H3T3 phosphorylation (Fig. 6c). While we cannot rule out the possibility that basic residues in the disordered N-terminal region of Haspin also contribute to chromatin binding, our results suggest that the observed interactions of the Haspin kinase domain with nucleosomal DNA is primarily responsible for the binding of this enzyme to chromatin. This mode of interaction is distinct from that of the histone kinase, VRK1, which contains an arginine-rich C-terminal tail that binds to the nucleosome acidic patch[46].

The molecular underpinnings and implications of the potentially specific binding of Haspin to the SHL 5.5/−2.5 DNA supergroove remain to be further delineated. Although our cryo-EM maps did not show Haspin bound to supergrooves that are too far to allow access to the tail of histone H3, we consider it likely that these nonproductive bound states occur transiently. Whereas these nonproductive states could be viewed as inhibitory, we favor a scenario in which binding of Haspin in alternative grooves constitutes a mechanism by which the nucleosome captures Haspin, allowing the enzyme to then dissociate and immediately rebind the correct groove and phosphorylate histone H3. This hypothesis is analogous to the 'facilitated diffusion' model, whereby the search of a transcription factor for its DNA binding site is facilitated by sampling nearby nonspecific sites and then hopping or sliding to the target sequence[47].

Are there other proteins that bind to nucleosome supergrooves? A Foldseek[48] search of the AlphaFold database for structures similar to the C-terminal kinase domain lobe of Haspin (610–798) identified seven structurally related human proteins, all of which are kinases: AKT1, CLK2, MAPK1, MAPK14, CLK4, MAPK3 and PINK1. Whereas Haspin's αH helix and αF–αH loop form extensive electrostatic interactions within the nucleosomal DNA supergroove (Fig. 2c), all seven related proteins have a shorter αH helix and repositioned αF–αH loop that would not permit a mode of DNA binding similar to Haspin (Fig. 7a). In addition, none of the structural homologs has an electropositive surface that would be required to bind to negatively charged DNA (Fig. 7b). The ability of Haspin to bind to a major DNA supergroove thus appears to be an adaptation of the conserved kinase domain to bind nucleosomes. Future structural and bioinformatics investigations should help to determine whether there are other chromatin-binding proteins that recognize the unique features of major and minor DNA supergrooves.

Online content

Any methods, additional references, Nature Portfolio reporting summaries, source data, extended data, supplementary information, acknowledgements, peer review information; details of author contributions and competing interests; and statements of data and code availability are available at https://doi.org/10.1038/s41594-025-01502-y.

References

1. Bannister, A. J. & Kouzarides, T. Regulation of chromatin by histone modifications. *Cell Res.* **21**, 381–395 (2011).
2. Wang, F. & Higgins, J. M. Histone modifications and mitosis: countermarks, landmarks, and bookmarks. *Trends Cell Biol.* **23**, 175–184 (2013).
3. Wilkins, B. J. et al. A cascade of histone modifications induces chromatin condensation in mitosis. *Science* **343**, 77–80 (2014).
4. Yamagishi, Y., Honda, T., Tanno, Y. & Watanabe, Y. Two histone marks establish the inner centromere and chromosome bi-orientation. *Science* **330**, 239–243 (2010).
5. Broad, A. J., DeLuca, K. F. & DeLuca, J. G. Aurora B kinase is recruited to multiple discrete kinetochore and centromere regions in human cells. *J. Cell Biol.* **219**, e201905144 (2020).
6. Polioudaki, H. et al. Mitotic phosphorylation of histone H3 at threonine 3. *FEBS Lett.* **560**, 39–44 (2004).
7. Qian, J., Lesage, B., Beullens, M., Van Eynde, A. & Bollen, M. PP1/Repo-man dephosphorylates mitotic histone H3 at T3 and regulates chromosomal aurora B targeting. *Curr. Biol.* **21**, 766–773 (2011).
8. Wang, F. et al. Histone H3 Thr-3 phosphorylation by Haspin positions Aurora B at centromeres in mitosis. *Science* **330**, 231–235 (2010).
9. Kelly, A. E. et al. Survivin reads phosphorylated histone H3 threonine 3 to activate the mitotic kinase Aurora B. *Science* **330**, 235–239 (2010).
10. Carmena, M., Wheelock, M., Funabiki, H. & Earnshaw, W. C. The chromosomal passenger complex (CPC): from easy rider to the godfather of mitosis. *Nat. Rev. Mol. Cell Biol.* **13**, 789–803 (2012).

11. Crosio, C. et al. Mitotic phosphorylation of histone H3: spatio-temporal regulation by mammalian Aurora kinases. *Mol. Cell. Biol.* **22**, 874–885 (2002).
12. Welburn, J. P. et al. Aurora B phosphorylates spatially distinct targets to differentially regulate the kinetochore–microtubule interface. *Mol. Cell* **38**, 383–392 (2010).
13. Dai, J. & Higgins, J. M. Haspin: a mitotic histone kinase required for metaphase chromosome alignment. *Cell Cycle* **4**, 665–668 (2005).
14. Dai, J., Sultan, S., Taylor, S. S. & Higgins, J. M. The kinase haspin is required for mitotic histone H3 Thr 3 phosphorylation and normal metaphase chromosome alignment. *Genes Dev.* **19**, 472–488 (2005).
15. Higgins, J. M. Haspin-like proteins: a new family of evolutionarily conserved putative eukaryotic protein kinases. *Protein Sci.* **10**, 1677–1684 (2001).
16. Higgins, J. Structure, function and evolution of haspin and haspinrelated proteins, a distinctive group of eukaryotic protein kinases. *Cell. Mol. Life Sci.* **60**, 446–462 (2003).
17. Wang, F. et al. Haspin inhibitors reveal centromeric functions of Aurora B in chromosome segregation. *J. Cell Biol.* **199**, 251–268 (2012).
18. Dai, J., Sullivan, B. A. & Higgins, J. M. Regulation of mitotic chromosome cohesion by Haspin and Aurora B. *Dev. Cell* **11**, 741–750 (2006).
19. Markaki, Y., Christogianni, A., Politou, A. S. & Georgatos, S. D. Phosphorylation of histone H3 at Thr3 is part of a combinatorial pattern that marks and configures mitotic chromatin. *J. Cell Sci.* **122**, 2809–2819 (2009).
20. Kawashima, S. A., Yamagishi, Y., Honda, T., Ishiguro, K.-I. & Watanabe, Y. Phosphorylation of H2A by Bub1 prevents chromosomal instability through localizing shugoshin. *Science* **327**, 172–177 (2009).
21. Liang, C. et al. Centromere-localized Aurora B kinase is required for the fidelity of chromosome segregation. *J. Cell Biol.* **219**, e201907092 (2020).
22. Hadders, M. A. et al. Untangling the contribution of Haspin and Bub1 to Aurora B function during mitosis. *J. Cell Biol.* **219**, e201907087 (2020).
23. Kang, T.-H. et al. Mitotic histone H3 phosphorylation by vaccinia-related kinase 1 in mammalian cells. *Mol. Cell. Biol.* **27**, 8533–8546 (2007).
24. Jeong, M.-W., Kang, T.-H., Kim, W., Choi, Y. H. & Kim, K.-T. Mitogen-activated protein kinase phosphatase 2 regulates histone H3 phosphorylation via interaction with vaccinia-related kinase 1. *Mol. Biol. Cell* **24**, 373–384 (2013).
25. Cartwright, T. N. et al. Dissecting the roles of Haspin and VRK1 in histone H3 phosphorylation during mitosis. *Sci. Rep.* **12**, 11210 (2022).
26. Quadri, R., Sertic, S. & Muzi-Falconi, M. Roles and regulation of Haspin kinase and its impact on carcinogenesis. *Cell. Signal.* **93**, 110303 (2022).
27. Eswaran, J. et al. Structure and functional characterization of the atypical human kinase haspin. *Proc. Natl Acad. Sci. USA* **106**, 20198–20203 (2009).
28. De Antoni, A., Maffini, S., Knapp, S., Musacchio, A. & Santaguida, S. A small-molecule inhibitor of Haspin alters the kinetochore functions of Aurora B. *J. Cell Biol.* **199**, 269–284 (2012).
29. Wotring, L. L. & Townsend, L. B. Study of the cytotoxicity and metabolism of 4-amino-3-carboxamido-1-(β-D-ribofuranosyl) pyrazolo [3, 4-d] pyrimidine using inhibitors of adenosine kinase and adenosine deaminase. *Cancer Res.* **39**, 3018–3023 (1979).
30. Fedorov, O. et al. A systematic interaction map of validated kinase inhibitors with Ser/Thr kinases. *Proc. Natl Acad. Sci. USA* **104**, 20523–20528 (2007).
31. Amoussou, N. G., Bigot, A., Roussakis, C. & Robert, J.-M. H. Haspin: a promising target for the design of inhibitors as potent anticancer drugs. *Drug Discov. Today* **23**, 409–415 (2018).
32. Tanaka, H. et al. Identification and characterization of a haploid germ cell-specific nuclear protein kinase (Haspin) in spermatid nuclei and its effects on somatic cells. *J. Biol. Chem.* **274**, 17049–17057 (1999).
33. Tanaka, H. et al. Cloning and characterization of human haspin gene encoding haploid germ cell-specific nuclear protein kinase. *Mol. Hum. Reprod.* **7**, 211–218 (2001).
34. Villa, F. et al. Crystal structure of the catalytic domain of Haspin, an atypical kinase implicated in chromatin organization. *Proc. Natl Acad. Sci. USA* **106**, 20204–20209 (2009).
35. Hanks, S. K. & Hunter, T. The eukaryotic protein kinase superfamily: kinase (catalytic) domain structure and classification 1. *FASEB J.* **9**, 576–596 (1995).
36. Maiolica, A. et al. Modulation of the chromatin phosphoproteome by the Haspin protein kinase. *Mol. Cell. Proteomics* **13**, 1724–1740 (2014).
37. Barski, A. et al. High-resolution profiling of histone methylations in the human genome. *Cell* **129**, 823–837 (2007).
38. Ghenoiu, C., Wheelock, M. S. & Funabiki, H. Autoinhibition and Polo-dependent multisite phosphorylation restrict activity of the histone H3 kinase Haspin to mitosis. *Mol. Cell* **52**, 734–745 (2013).
39. Jumper, J. et al. Highly accurate protein structure prediction with AlphaFold. *Nature* **596**, 583–589 (2021).
40. Zhou, L., Tian, X., Zhu, C., Wang, F. & Higgins, J. M. Polo-like kinase-1 triggers histone phosphorylation by Haspin in mitosis. *EMBO Rep.* **15**, 273–281 (2014).
41. Goto, Y. et al. Pds5 regulates sister-chromatid cohesion and chromosome bi-orientation through a conserved protein interaction module. *Curr. Biol.* **27**, 1005–1012 (2017).
42. Horn, V. & van Ingen, H. *Recognition of Nucleosomes by Chromatin Factors: Lessons from Data-Driven Docking-Based Structures of Nucleosome–Protein Complexes* (IntechOpen, 2018).
43. McGinty, R. K. & Tan, S. Recognition of the nucleosome by chromatin factors and enzymes. *Curr. Opin. Struct. Biol.* **37**, 54–61 (2016).
44. Kale, S., Goncearenco, A., Markov, Y., Landsman, D. & Panchenko, A. R. Molecular recognition of nucleosomes by binding partners. *Curr. Opin. Struct. Biol.* **56**, 164–170 (2019).
45. Edayathumangalam, R. S., Weyermann, P., Gottesfeld, J. M., Dervan, P. B. & Luger, K. Molecular recognition of the nucleosomal 'supergroove. *Proc. Natl Acad. Sci. USA* **101**, 6864–6869 (2004).
46. Budziszewski, G. R. et al. Multivalent DNA and nucleosome acidic patch interactions specify VRK1 mitotic localization and activity. *Nucleic Acids Res.* **50**, 4355–4371 (2022).
47. Berg, O. G., Winter, R. B. & von Hippel, P. H. Diffusion-driven mechanisms of protein translocation on nucleic acids. 1. Models and theory. *Biochemistry* **20**, 6929–6948 (1981).
48. van Kempen, M. et al. Fast and accurate protein structure search with Foldseek. *Nat. Biotechnol.* **42**, 243–246 (2024).

Methods

Expression and purification of histones

Expression plasmids for *Xenopus laevis* histones H2A, H2B, H3 and H4 were a gift from Greg Bowman (Johns Hopkins University). Histones were expressed and purified as previously described[49], with the following modifications. Thawed cell pellet was lysed with multiple passes through a Microfluidizer (Microfluidics). After lysis, centrifugation and multiple washes using a buffer containing Triton X-100, washed cell pellets were resuspended in a buffer containing 20 mM HEPES pH 7.5, 7 M guanidine HCl and 10 mM dithiothreitol (DTT). Resuspended washed cell pellets were size exclusion purified using a buffer containing 10 mM Tris pH 8.0, 7 M urea, 1 mM EDTA and 5 mM β-mercaptoethanol (BME). Fractions were pooled and injected onto a two-column series with a HiTrap Q-XL column connected upstream of a HiTrap SP-XL column using a buffer containing 20 mM Tris pH 7.8, 7 M urea, 1 mM EDTA and 5 mM BME). The Q-XL column was removed from the system, and then the histones were eluted from the SP-XL column with a gradient of 0–1 M NaCl on an ÄKTA Pure (Cytiva) chromatography system.

Purification of Widom 601 DNA

The Widom 601 DNA sequence (147 bp)[50] was expressed in *Escherichia coli* strain XL-1 Blue using the pST55-16×601 plasmid[51]. The 601 sequence was expressed, purified and isolated as described[52]. The 601 sequence used is

5′-ATCGGATGTATATATCTGACACGTGCCTGGAGACTAGGGAG
TAATCCCCTTGGCGGTTAAAACGCGGGGGACAGCGCGTACGT
GCGTTTAAGCGGTGCTAGAGCTGTCTACGACCAATTGAGCGGC
CTCGGCACCGGGATTCTCGAT-3′.

The Widom 601 DNA flanked by 19 bp of linker DNA at each end (185 bp) was amplified using polymerase chain reaction (PCR) using primers (IDT DNA) containing 19-bp overhanging regions using the linear double-stranded 147 bp 601 DNA as a template. One primer contained a biotin tag to allow for the amplification of biotinylated 185 bp DNA. The primers used were as follows.

Forward:
5′-biosg-GTCGCTGTTCGCGACCGGCAATCGATGTATATATCT
GACACGTGCC-3′

Reverse:
5′-GACCCTATACGCGGCCGCCCATCAGAATCCCGGTGCCGAG-3′

Phusion polymerase was used to amplify the reaction in 100 µl reaction volumes using standard PCR parameters. The PCR product mixture was precipitated by combining 100% ethanol (EtOH), PCR product mixture and 3 M sodium acetate pH 5.2 in a 10:1:20 ratio and placing the mixture at −80 °C for 1 h. The precipitated PCR product mixture was then centrifuged and the supernatant removed. The pellet was washed with 70% EtOH, centrifuged, the supernatant removed, and the pellet allowed to dry. The pellet was resuspended in TE buffer (10 mM Tris pH 8.0 and 1 mM EDTA). A phenol:chloroform:isoamyl alcohol solution 25:24:1 was added to an equal volume of resuspended PCR product pellet, vortexed and centrifuged to separate the phases. The organic phase was removed, and the aqueous phase was extracted twice more the same way. All the removed organic phases were pooled and back-extracted with TE buffer to collect any PCR product left behind in the organic phase, and all the aqueous phases were combined and saved as the purified PCR product. Purified PCR product, 3 M sodium acetate pH 5.2 and 100% EtOH was combined in a 10:1:20 ratio and placed at −20 °C overnight. The precipitated purified PCR product was then centrifuged, and the pellet was washed with 70% EtOH, centrifuged again and allowed to dry. This pellet of purified 185 bp 601 DNA was then resuspended in MilliQ (Sigma) water and stored at −20 °C.

Preparation of nucleosomes

Unmodified nucleosome (185 bp) was reconstituted as previously described[49], with the following modifications.

For each nucleosome sample, histone octamer and Widom 601 DNA was combined in an octamer:DNA molar ratio of 1.2:1 in a buffer containing 10 mM Tris pH 7.5, 2 M KCl, 1 mM EDTA and 1 mM DTT, such that the final DNA concentration was 6 µM. The salt concentration was gradually reduced to 0.25 M KCl over 24 h by salt gradient dialysis to assemble the nucleosome. Precipitate was removed by centrifugation, and the purity of the nucleosome sample was assessed using an EMSA. If the nucleosome sample showed excess free DNA or higher-order species, it was further purified by loading onto a SK DEAE-5PW column (TOSOH Biosciences) using a buffer containing 10 mM Tris pH 7.5, 0.25 M KCl, 0.5 mM EDTA and 1 mM DTT and eluted with a gradient of 0.25–0.6 M KCl on an Agilent HPLC instrument. Purified nucleosome was dialyzed into a buffer containing 20 mM HEPES pH 7.5, 25 mM KCl, 1 mM EDTA, 1 mM DTT and 20% glycerol, flash-frozen in liquid nitrogen and stored at −80 °C.

For tailless nucleosome EMSAs, canonical unmodified nucleosomes (199 bp) (Epicypher, 16-2044) and tailless unmodified nucleosomes (Epicypher, 16-2027) were purchased from Epicypher.

Purification of Haspin and Haspin mutants

Haspin plasmid construct (GSG2) was a gift from Nicola Burgess-Brown (Addgene plasmid no. 38915; http://n2t.net/addgene:38915; RRID: Addgene_38915). This construct was used to create Haspin mutant constructs using around-the-horn mutagenesis. The original Addgene wild-type Haspin construct or Haspin mutant constructs encoding Haspin (465–798) fused to an N-terminal hexahistidine tag (6×His) and tobacco etch virus (TEV) protease cut site, were transformed into BL21(DE3)Rosetta2-pLysS *E. coli* cells. The colonies were used to inoculate 5 ml volumes of medium, which were expanded to larger 1 l volumes of medium for the full-scale growth. Cultures were grown at 37 °C and 200 rpm in 2× yeast extract tryptone medium supplemented with kanamycin and chloramphenicol. Cultures were induced by addition of 1 mM isopropyl-β-D-thiogalactopyranoside when the culture reached an OD_{600} of 0.4 and were grown for an additional 16 h at 18 °C. The cells were collected by centrifugation and the pellets resuspended in a buffer containing 20 mM HEPES pH 7.5, 300 mM NaCl, 40 mM imidazole, 5 mM BME and one tablet per 50 ml of complete protease inhibitor (Roche, 11836153001), flash-frozen in liquid nitrogen and stored at −80 °C.

The frozen cell pellet suspensions were thawed in a water bath, and an equal volume of buffer containing 20 mM HEPES pH 7.5, 300 mM NaCl, 40 mM imidazole, 1 mM DTT and 0.2 mM phenylmethylsulfonyl fluoride (PMSF) was added. The diluted cell suspensions were lysed by sonication for three rounds each of 1 min total processing time (5 s on, 10 s off) at 40% power. The resulting whole-cell extracts were centrifuged at about 35,000*g*, and the supernatants were filtered using a 1.1 µm filter to obtain clarified extracts. Clarified extracts were loaded onto a 5 ml HisTrap HP (Cytiva) column equilibrated in 20 mM HEPES pH 7.5, 300 mM NaCl, 40 mM imidazole, 1 mM DTT and 0.2 mM PMSF and eluted with a gradient of 0.04–1 M imidazole on an ÄKTA Pure instrument (Cytiva). The eluted proteins were diluted with 20 mM HEPES pH 7.5, 1 mM DTT and 0.2 mM PMSF to a final salt concentration of 150 mM NaCl and filtered using a 1.1 µm filter. Eluted Haspin mutant containing four charge-reversal mutations (K659E, K759E, K761E and R772E) was diluted to a final salt concentration of 50 mM NaCl and filtered using a 1.1 µm filter. The filtered proteins were loaded onto a 5 ml HiTrap heparin (Cytiva) column equilibrated in 20 mM HEPES pH 7.5, 50 mM NaCl, 1 mM DTT and 0.2 mM PMSF and eluted with a gradient of 0.15–2 M NaCl on an ÄKTA Pure instrument. The Haspin mutant containing four charge-reversal mutations was eluted from the heparin column with a gradient of 0.05–2 M NaCl. The eluted proteins were dialyzed overnight in a buffer

containing 20 mM HEPES pH 7.5, 150 mM NaCl, 10% glycerol, 1 mM DTT and 0.2 mM PMSF, concentrated, flash-frozen in liquid nitrogen and stored at −80 °C.

Cryo-EM sample preparation

Wild-type Haspin (465–798) containing an N-terminal 6×His tag and TEV protease cleavage site was thawed on ice and mixed with nucleosome containing 147 bp 601 Widom DNA with 19 bp linkers (185 bp) to a final concentration of 8 µM Haspin and 4 µM nucleosome in a buffer containing 20 mM HEPES pH 7.5, 150 mM KCl and 1 mM DTT. The mixture was incubated on ice for 30 min. Quantifoil R 1.2/1.3 gold 300 mesh grids (Electron Microscopy Sciences, Q350AR1.3) were glow-discharged for 45 s at 15 mA using a PELCO easiGLOW Glow Discharge System to apply a negative charge to their surface. Then, 3 µl of sample mixture was applied to the grid, immediately blotted for 4.5 s with a blot force of 3 and plunge-frozen in liquid ethane using a Vitrobot Mark IV apparatus (Thermo Fisher) set to 100% humidity and 4 °C.

Cryo-EM data collection

To evaluate the feasibility of determining the cryo-EM structure of Haspin bound to nucleosome without using crosslinker, a small cryo-EM dataset of Haspin bound to nucleosome was collected at the Beckman Center for Cryo-EM at the Johns Hopkins University School of Medicine using a Thermo Fisher Glacios 200 kV electron microscope equipped with a Falcon 4i direct electron detector. A dataset of 1,026 exposures was collected using Thermo Fisher E Pluribus Unum (EPU) in counting mode and recorded in Electron Event Representation (EER) format using a magnification of ×120,000, pixel size of 1.19 Å, nominal dose of 40 e^- $Å^{-2}$, dose rate of 6.69 e^- per pixel per second and defocus range of −0.5 to −2.5 µm. The final processed EM density map derived from this dataset was used to generate two-dimensional (2D) templates for use during data processing of the large cryo-EM dataset of Haspin bound to nucleosome, which was collected using a Thermo Fisher Titan Krios 300 kV electron microscope.

A large cryo-EM dataset for determining the high-resolution structure of Haspin bound to nucleosome was collected at the Beckman Center for Cryo-EM at the Johns Hopkins University School of Medicine using a Titan Krios at 300 kV equipped with a Falcon 4 direct electron detector and Selectris energy filter. A dataset of 9,999 exposures was collected using Thermo Fisher EPU in counting mode and recorded in EER format using a magnification of ×130,000, pixel size of 0.97 Å, nominal dose of 40 e^- $Å^{-2}$, dose rate of 7.74 e^- per pixel per second, defocus range of −0.5 to −2.5 µm and energy filter slit width of 10 eV. A multishot imaging strategy was used to collect three shots per hole, utilizing beam image shift to move between each target.

Cryo-EM data processing

The dataset was processed in cryoSPARC v4.2 (refs. 53,54). Exposures were imported with an EER upsampling factor of 2 and cropped to one-half their original resolution using patch motion correction. The contrast transfer function (CTF) correction was performed with 'patch CTF estimation'. Poor-quality micrographs were removed using 'manually curate exposures', yielding 9,362 high-quality micrographs. A set of low-pass filtered 2D templates from the test dataset of Haspin bound to nucleosome were used to perform particle picking using 'template picker' and 'inspect picks', then extracted using 'extract from micrographs' to yield an uncleaned particle stack (6,762,618 particles). One round of '2D classification' and 'select 2D classes' was performed to remove junk particles by discarding distinctly poor-quality 2D classes to yield a partially cleaned particle stack (2,249,799 particles). Multiple parallel multi-structure ab-initio reconstruction jobs were performed to produce one good 3D class and three poor 3D classes for subsequent heterogeneous refinement particle cleaning. Particle cleaning was performed using four parallel four-structure heterogeneous refinement jobs, using the one good 3D class and three poor 3D classes derived from the previous ab-initio reconstruction job as inputs for the refinement. This parallel heterogeneous refinement particle cleaning step was repeated two additional times, keeping the particles from the good classes for each subsequent cleaning steps, yielding a cleaned particle stack of 900,411 particles. The cleaned particle stack was reextracted and recentered using aligned shifts. Ab-initio reconstruction and homogeneous refinement jobs were performed to produce a structure showing some low-resolution speckles of EM density on the periphery of the nucleosomal DNA in two places on opposite sides of the nucleosome adjacent to the histone H3 tail. Focused 3D classification was performed with a single mask file containing combined two spherical mask volumes each centered on one the two areas of speckled EM density. The output volumes showed structures of free nucleosome and structures of Haspin bound to nucleosome. The particles corresponding to Haspin bound to nucleosome were selected and refined with homogeneous refinement, then local refinement. A second round of focused 3D classification was performed with a spherical mask centered on the Haspin density to produce structures of Haspin bound to nucleosome in two positions. Individual particle CTF was refined with local CTF refinement, image group CTF was refined with global CTF refinement, and the structures were refined with local refinement to produce Haspin bound to nucleosome in position 1 (152,199 particles, 3.01 Å) and Haspin bound to nucleosome in position 2 (154,151 particles, 2.99 Å).

Cryo-EM model building and refinement

Initial models of Haspin bound to nucleosome were constructed by using rigid body fitting of models for an unmodified nucleosome (PDB: 4ZUX)[55] and Haspin (PDB: 4OUC)[36] into EM density maps using in ChimeraX[56] and then refined using all-atom flexible refinement with strong restraints in Coot 0.9.6 (ref. 57). All waters, ions and small molecules were stripped from the original structures so that only the atoms corresponding to nucleosome and Haspin could be used for model building. Histone tails were extended where density was visible, and the nucleosomal DNA was extended from 147 bp to 157 bp to account for the extranucleosomal linker DNA present in this sample. The modeled Haspin includes residues 470–798. The models were further refined in PHENIX[58] using phenix.real_space_refine[59] and validated using the cryo-EM Comprehensive Validation module in PHENIX running MolProbity[60]. Figures were generated with ChimeraX[56].

EMSAs

Binding reactions were prepared in 12 µl volumes by combining Haspin and nucleosome in binding buffer (20 mM HEPES pH 7.6, 150 mM NaCl, 5% glycerol and 1 mM DTT). Nucleosomes were always added last. Prepared reactions were incubated on ice for 30 min to allow them to come to equilibrium. Before sample loading, 6% Tris–borate–EDTA (TBE) gels were equilibrated by running at 150 V for 60 min at 4 °C in 0.25× TBE buffer. Then, 10 µl of each equilibrated binding reaction was loaded on the prepared gel and run at 150 V for 90 min at 4 °C in 0.25× TBE buffer. Gels were stained in the dark on a rotating shaker for 20 min with SYBR Gold (Invitrogen) DNA-intercalating stain diluted to 1:5,000, then imaged.

Immunoblotting activity assays

Assays to test wild-type Haspin (465–798) and Haspin mutants (465–798) histone H3 threonine 3 (H3T3) phosphorylation activity were prepared in 20 µl volumes by combining Haspin and nucleosome in kinase buffer (20 mM HEPES pH 7.6, 150 mM KCl, 1 mM $MgCl_2$, 1 mM DTT, 100 µM ATP and 0.25 mg ml^{-1} bovine serum albumin (GoldBio, A-420-250)). Nucleosomes were added last to initiate the reactions, which were incubated at room temperature. Time points at 5, 15 and 45 min were collected by quenching 6 µl of each reaction in 1.5× lithium dodecyl sulfate sample buffer. Before sample loading, quenched reactions were separated on a 4–12% Bis-Tris Gel (Thermo Fisher) by

SDS–PAGE, then transferred onto polyvinylidene difluoride membrane using a Trans-Blot Turbo Transfer System (Bio-Rad). Membranes were blocked with 5% milk in 1× Tris-buffered saline with 0.1% Tween-20 (TBST) buffer, probed with 1:5,000 anti-H3T3ph (Sigma-Aldrich, 04-746) or 1:5,000 anti-H3 (Abcam, ab1791) primary antibodies in 5% milk in 1× TBST overnight at 4 °C, then probed with 1:5,000 anti-rabbit (Invitrogen, 31460) horseradish-peroxidase-conjugated secondary antibody in 5% milk in 1× TBST for 1 h at room temperature. Membranes were stained with enhanced chemiluminescence reagent and imaged.

Cell lines and culture conditions

HEK293T cells were grown in Dulbecco's modified Eagle medium (Corning Cellgro) containing 10% fetal bovine serum (Sigma), 100 U ml^{-1} penicillin, 100 U ml^{-1} streptomycin and 2 mM L-glutamine and were maintained at 37 °C in a 5% CO_2 atmosphere with 21% oxygen.

Fluorescence microscopy

For fluorescence microscopy experiments, cells were grown to 75% confluency in a six-well dish, then transfected with pcDNA5/FRT plasmids (Invitrogen, V601020) expressing either EGFP alone, EGFP–Haspin (WT) or EGFP–Haspin (K659E, K759E, K761E and R772E) using Lipofectamine LTX transfection reagent (Thermo Fisher, 15338500). Cells were transferred to 12-mm glass coverslips the day after and were fixed in methanol at −20 °C for 10 min on the third day. DNA was stained with DAPI in phosphate-buffered saline (PBS), and cells were mounted with ProLong Gold Antifade reagent (Invitrogen).

Imaging was performed using a Zeiss Axio Observer 7 inverted microscope with Slidebook 2023 software (3i—Intelligent, Imaging Innovations), CSU-W1 (Yokogawa) T1 50 µm Spinning Disk and Prime 95B CMOS camera (Teledyne Photometrics) with a 63× plan-apochromat oil immersion objective with 1.4 numerical aperture. Mitotic cells were imaged with 0.25 µm *z* sections, deconvolved using the Slidebook Microvolution algorithm, and maximum intensity projected before analysis. Using FIJI software[61], mitotic chromosome regions were established from the DAPI channel, and median EGFP signal intensity was measured within the chromosome region ($EGFP_{DNA}$) and for a 1-µm-wide cytoplasmic ribbon surrounding the DNA ($EGFP_{CYTO}$). The ratio of intensity measurements was reported on a $\log_2$ scale and plotted in GraphPad Prism.

Immunoblotting cellular assays

For cellular assays gauging the effect of Haspin overexpression in HEK293T cells, cells were split to ~30% confluency in a six-well dish. After 24 h, each well was transfected with 10 µg of EGFP only, EGFP–Haspin (WT) or EGFP-Haspin (K659E, K759E, K761E and R772E) using Lipofectamine 3000 (Thermo Fisher, L3000008), following the manufacturer's protocol. After 24 h, the cells were visualized for GFP expression. The cells were washed with ice-cold PBS twice, detached using 0.25% trypsin–EDTA and then collected by spinning at 500*g* for 5 min. The supernatant was removed, and the cells were washed again with PBS before being resuspended in 250 µl of ice-cold PBS.

Core histones were extracted using a histone extraction kit (Active Motif, 40028), following the manufacturer's instructions. Histone extracts were separated on a 4–12% Bis-Tris Gel (Thermo Fisher) by SDS–PAGE, then transferred onto polyvinylidene difluoride membrane using a Trans-Blot Turbo Transfer System (Bio-Rad). Membranes were blocked with 5% milk in 1× TBST buffer, probed with 1:2,500 anti-H3T3ph (Sigma-Aldrich, 04-746) or 1:2,500 anti-H3 (Abcam, ab1791) primary antibodies in 5% milk in 1× TBST overnight at 4 °C, then probed with 1:5,000 anti-rabbit (Invitrogen, 31460) horseradish-peroxidase-conjugated secondary antibody in 5% milk in 1× TBST for 1 h at room temperature. Membranes were stained with enhanced chemiluminescence reagent and imaged.

Foldseek protein structure homology search

The Foldseek[48] Search Web Server (https://search.foldseek.com/search) was used with default parameters to search for structurally homologous proteins in the AlphaFold proteome. The C-terminal lobe of the Haspin kinase domain (residues 610–798) from the structure of Haspin bound to nucleosome in position 1 was used as a search query, and the results were filtered to include only human proteins.

Reporting summary

Further information on research design is available in the Nature Portfolio Reporting Summary linked to this article.

Data availability

Models and cryo-EM maps were deposited in the PDB and Electron Microscopy Data Bank (EMDB) under the following accession codes: Haspin position 1 (PDB: 9B2S, EMDB: 44113), Haspin position 2 (PDB: 9B2T, EMDB: 44114) and Haspin local refinement (PDB: 9B2U, EMDB: 44115). Raw cryo-EM movies were deposited in the EMPIAR database under the accession code EMPIAR-11971. Source data are provided with this paper.

References

49. Luger, K., Rechsteiner, T. J. & Richmond, T. J. in *Methods in Enzymology* Vol. 304, 3–19 (Elsevier, 1999).
50. Lowary, P. & Widom, J. New DNA sequence rules for high affinity binding to histone octamer and sequence-directed nucleosome positioning. *J. Mol. Biol.* **276**, 19–42 (1998).
51. Makde, R. D., England, J. R., Yennawar, H. P. & Tan, S. Structure of RCC1 chromatin factor bound to the nucleosome core particle. *Nature* **467**, 562–566 (2010).
52. Dyer, P. N. et al. in *Methods in Enzymology* Vol. 375, 23–44 (Elsevier, 2003).
53. Punjani, A., Rubinstein, J. L., Fleet, D. J. & Brubaker, M. A. cryoSPARC: algorithms for rapid unsupervised cryo-EM structure determination. *Nat. Methods* **14**, 290–296 (2017).
54. Punjani, A., Zhang, H. & Fleet, D. J. Non-uniform refinement: adaptive regularization improves single-particle cryo-EM reconstruction. *Nat. Methods* **17**, 1214–1221 (2020).
55. Morgan, M. T. et al. Structural basis for histone H2B deubiquitination by the SAGA DUB module. *Science* **351**, 725–728 (2016).
56. Pettersen, E. F. et al. UCSF ChimeraX: structure visualization for researchers, educators, and developers. *Protein Sci.* **30**, 70–82 (2021).
57. Emsley, P., Lohkamp, B., Scott, W. G. & Cowtan, K. Features and development of Coot. *Acta Crystallogr. Sect. D* **66**, 486–501 (2010).
58. Liebschner, D. et al. Macromolecular structure determination using X-rays, neutrons and electrons: recent developments in Phenix. *Acta Crystallogr. Sect. D* **75**, 861–877 (2019).
59. Afonine, P. V. et al. Real-space refinement in PHENIX for cryo-EM and crystallography. *Acta Crystallogr. Sect. D* **74**, 531–544 (2018).
60. Williams, C. J. et al. MolProbity: more and better reference data for improved all-atom structure validation. *Protein Sci.* **27**, 293–315 (2018).
61. Schindelin, J. et al. Fiji: an open-source platform for biological-image analysis. *Nat. Methods* **9**, 676–682 (2012).

Acknowledgements

We thank D. Sousa, D. Ding and K. Cai for their support with cryo-EM sample preparation and data collection at the Beckman Center for Cryo-EM at Johns Hopkins School of Medicine. We thank the Summer Academic Research Experience (SARE) Program at Johns Hopkins for providing support to host S.J.V. for a summer research

experience in the Wolberger lab. We thank the Wolberger lab for their insights and discussions on the paper. This work was supported by National Institute of General Medical Sciences grants R35GM130393 (C.W.), R01GM133897 (A.J.H.) and R01GM114119 (A.J.H.) and National Cancer Institute grants F31CA261154 (C.W.H.), F31CA271743 (S.R.) and R01CA266199 (A.J.H.) of the National Institutes of Health, and by a National Science Foundation Graduate Research Fellowship (A.S.E.).

Author contributions

C.W.H. performed cryo-EM data processing, structural modeling, map interpretation and in vitro experiments to assay Haspin binding and activity on canonical nucleosomes. C.R.G. performed cell-based experiments on Haspin localization. S.R. assayed Haspin phosphorylation of H3T3 on free histone H3 in vitro and on chromatin in cells. X.Z. prepared Haspin kinase domain mutant plasmid constructs. A.S.E. assayed Haspin binding to tailless nucleosomes. S.J.V. froze and clipped cryo-EM grids for data collection. A.J.H. oversaw execution and interpretation of cell-based experiments. C.W. oversaw all aspects of structure determination, biochemistry and data interpretation. C.W.H. and C.W. wrote the paper, with contributions and feedback from all other authors.

Competing interests

The authors declare no competing interests.

Additional information

Extended data is available for this paper at https://doi.org/10.1038/s41594-025-01502-y.

Supplementary information The online version contains supplementary material available at https://doi.org/10.1038/s41594-025-01502-y.

Correspondence and requests for materials should be addressed to Cynthia Wolberger.

Peer review information *Nature Structural & Molecular Biology* thanks the anonymous reviewers for their contribution to the peer review of this work. Peer reviewer reports are available. Primary Handling Editors: Sara Osman and Dimitris Typas, in collaboration with the *Nature Structural & Molecular Biology* and team.

https://doi.org/10.1038/s41594-025-01502-y

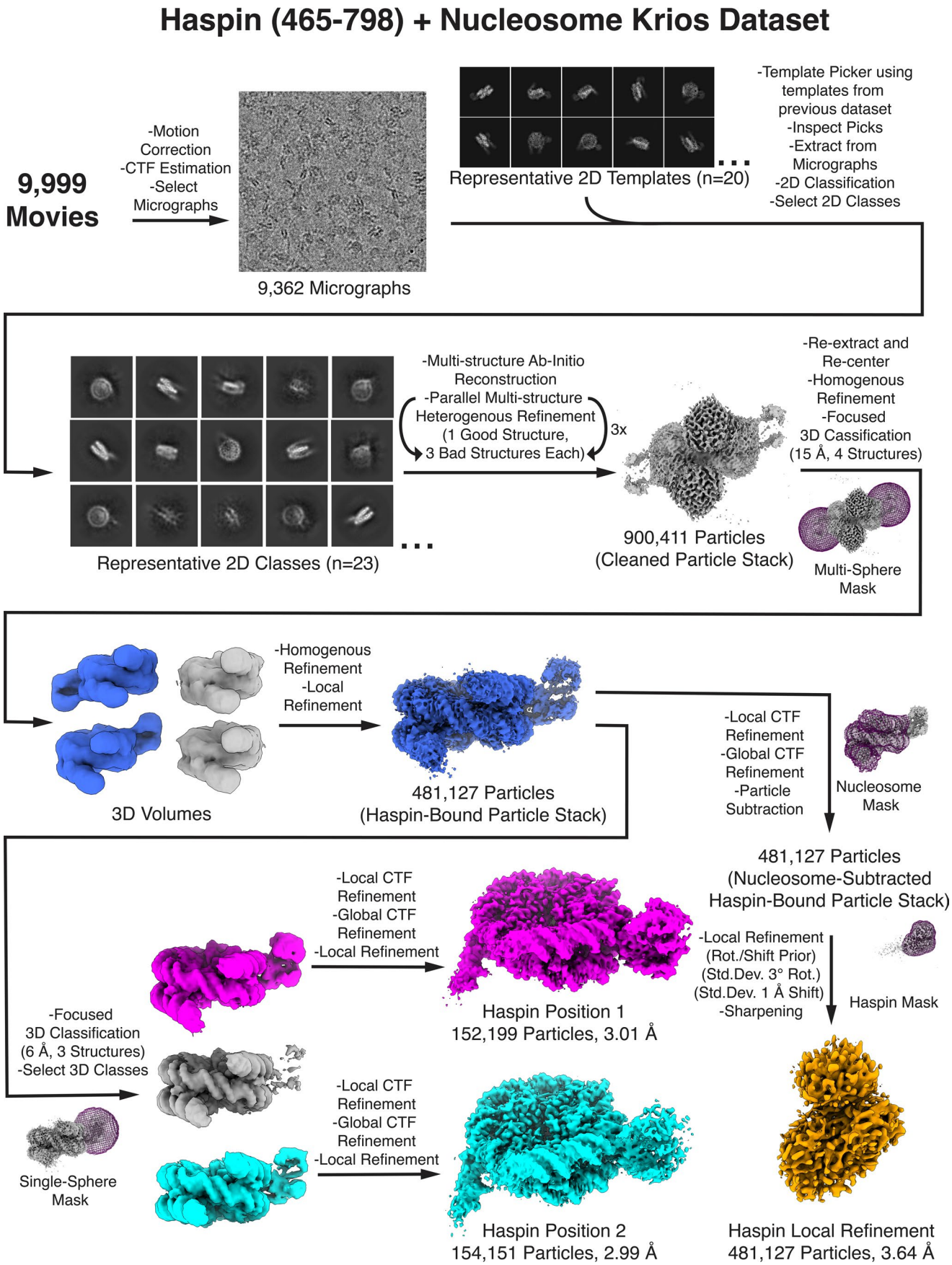

Extended Data Fig. 1 | Cryo-EM data processing workflow for Haspin (465-798) bound to nucleosome. General processing pipeline to obtain the final cryoEM maps of Haspin Position 1, Haspin Position 2, and Haspin Local Refinement.

https://doi.org/10.1038/s41594-025-01502-y

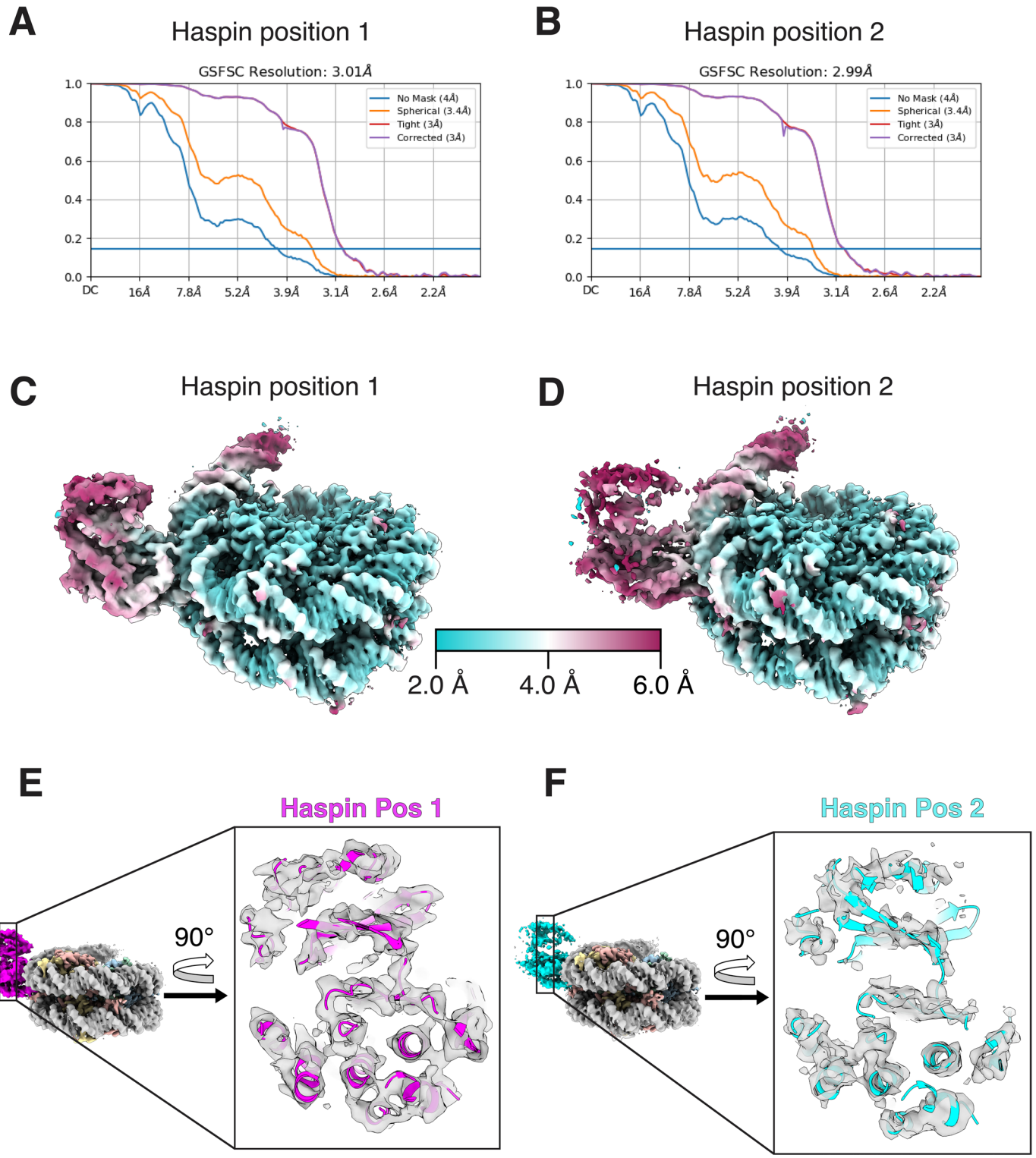

Extended Data Fig. 2 | Global and local resolution evaluation of both cryo-EM maps. a, b) Fourier Shell Correlation (FSC) plots using gold-standard 0.143 cutoffs for both cryo-EM maps of Haspin bound to nucleosome, **a**) position 1, **b**) position 2. **c, d**) Local resolution estimation color depictions for both cryo-EM maps corresponding to Haspin bound to nucleosome, **c**) position 1, **d**) position 2. **e, f**) Cut-away slice view through the center of both Haspin cartoon models showing the fit to their respective cryo-EM maps, **e**) position 1, **f**) position 2.

https://doi.org/10.1038/s41594-025-01502-y

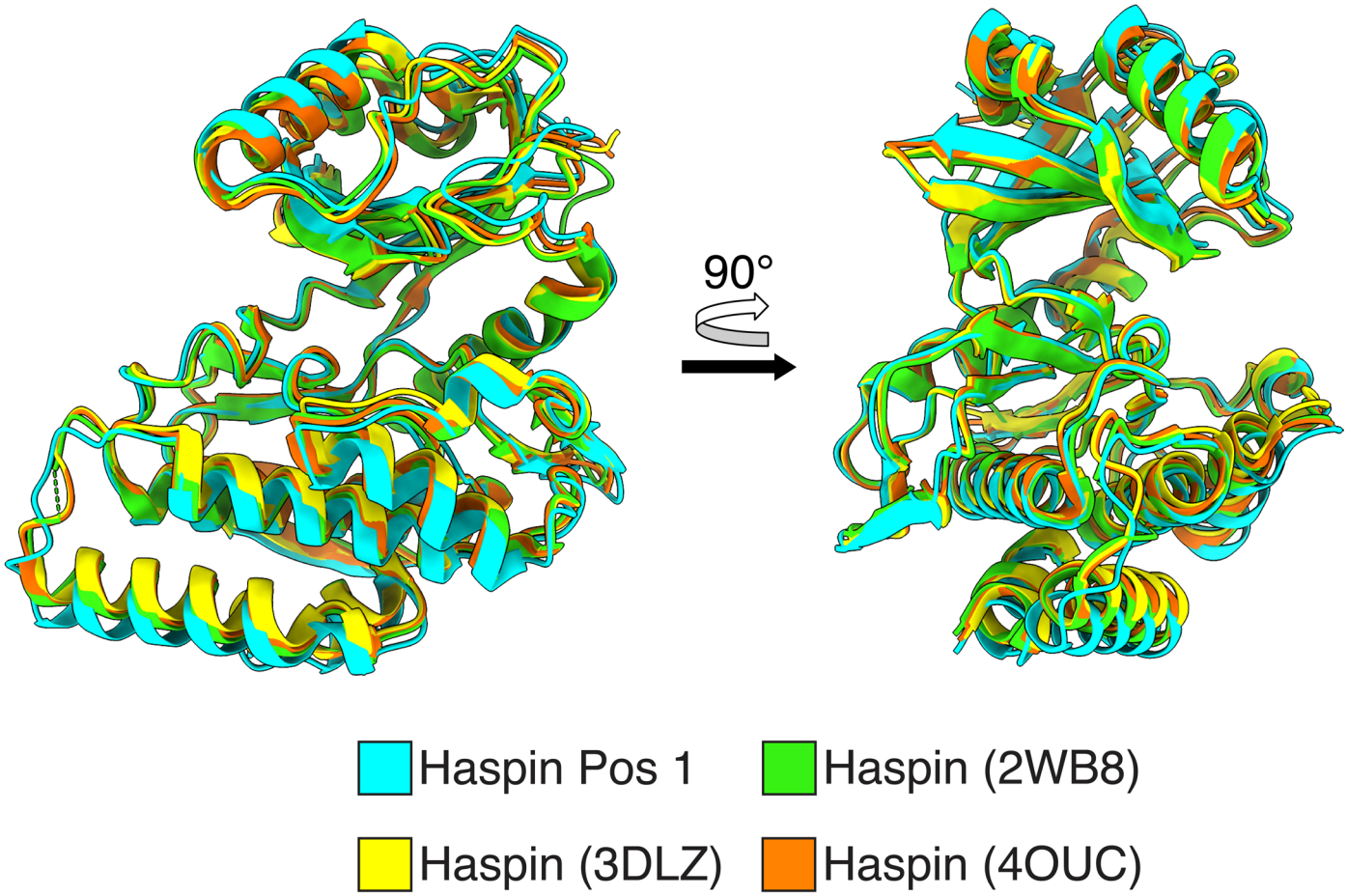

Extended Data Fig. 3 | Haspin structural alignments. Structural alignments of cartoon model of Haspin (470-798) in position 1 over Haspin (468-798) (PDB: 2WB8)[34], Haspin (470-798) (PDB: 3DLZ)[27], and Haspin (470-798) (PDB: 4OUC)[36].

https://doi.org/10.1038/s41594-025-01502-y

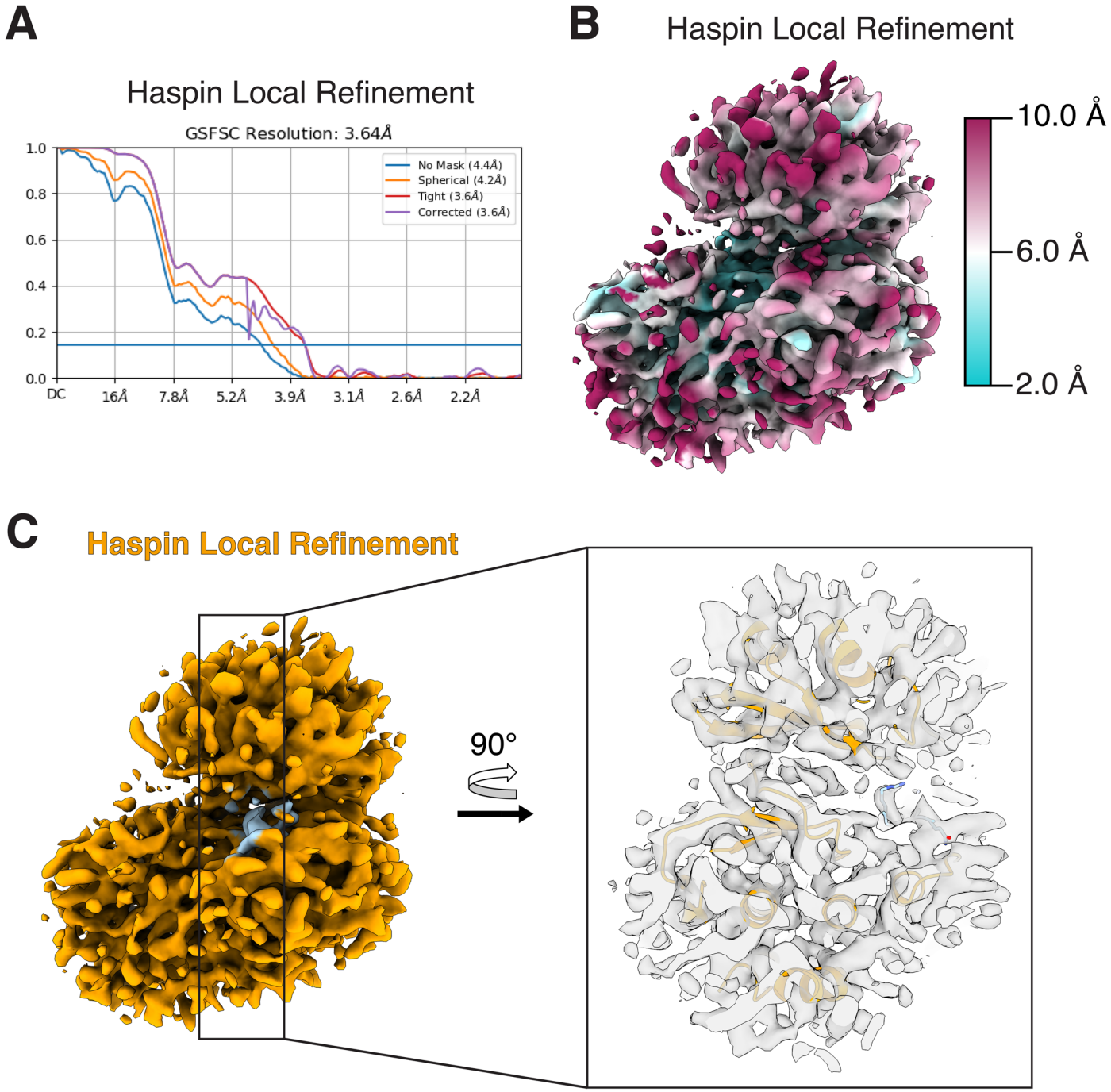

Extended Data Fig. 4 | Global and local resolution evaluation of Haspin local refinement cryo-EM map. a) Fourier Shell Correlation (FSC) plot using fold-standard 0.143 cutoffs for the Haspin local refinement cryo-EM map of Haspin bound to nucleosome. **b**) Local resolution estimation color depictions for the Haspin local refinement cryo-EM map of Haspin bound to nucleosome. **c**) Cut-away slice view through the center of Haspin showing the fit of the model to the cryo-EM map.

https://doi.org/10.1038/s41594-025-01502-y

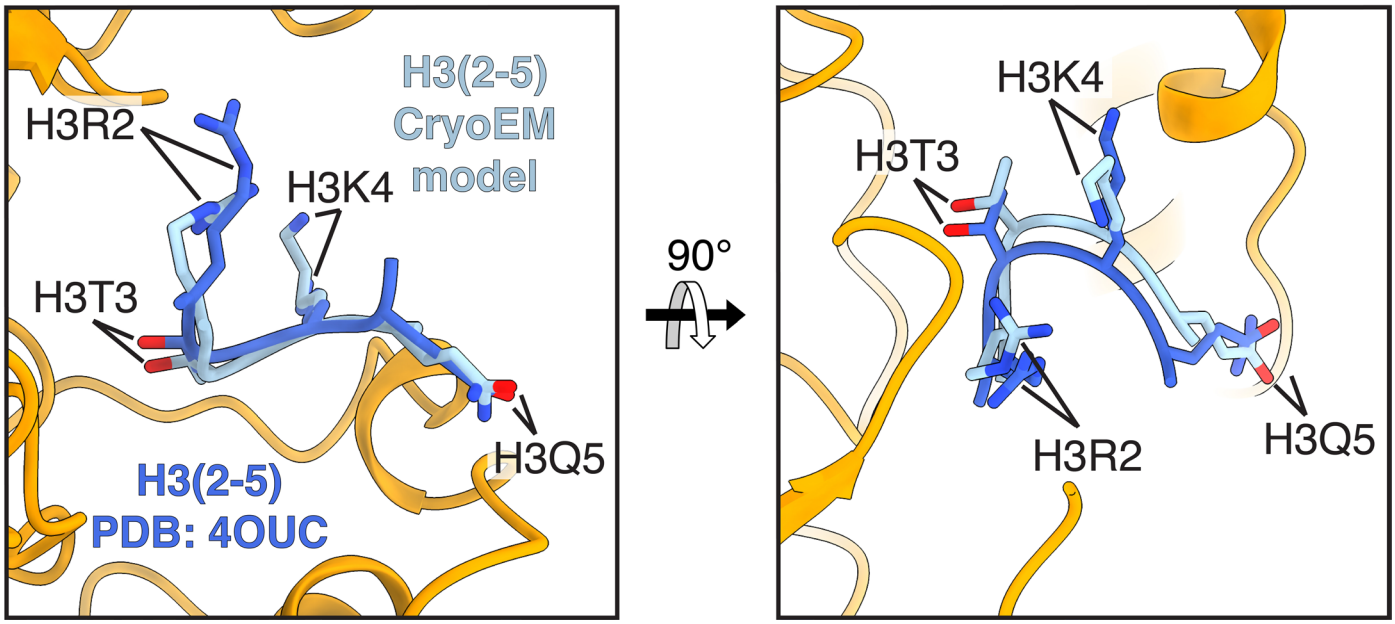

Extended Data Fig. 5 | Cryo-EM structure of H3 tail bound to Haspin is similar to crystal structure of H3 peptide bound to Haspin. A previously reported crystal structure of Haspin (PDB: 4OUC)[36] with bound H3 peptide (royal blue) was superimposed over our cryo-EM map of locally-refined Haspin (orange) containing bound H3 tail (light blue). Structures are depicted in cartoon and atom representation and show the similarity in the binding position of H3.

https://doi.org/10.1038/s41594-025-01502-y

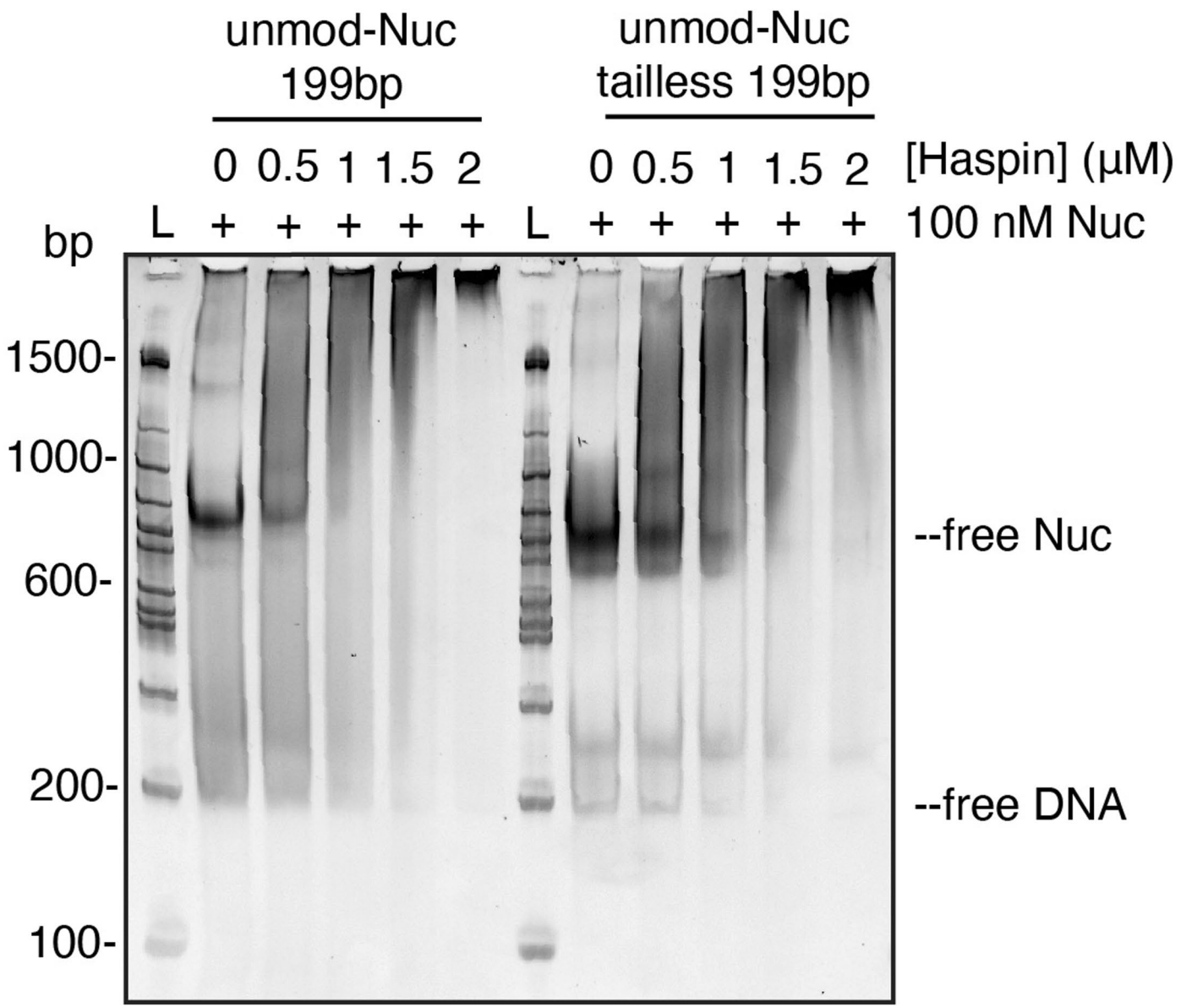

Extended Data Fig. 6 | Haspin binding to canonical and tailless nucleosome. Electrophoretic mobility shift assay (EMSA) showing binding of wild-type Haspin (465-798) to canonical unmodified nucleosome (199 bp) and tailless unmodified nucleosome (199 bp) at the indicated concentrations.

nature portfolio

Corresponding author(s): Cynthia Wolberger

Last updated by author(s): Jan 4, 2024

Reporting Summary

Nature Portfolio wishes to improve the reproducibility of the work that we publish. This form provides structure for consistency and transparency in reporting. For further information on Nature Portfolio policies, see our Editorial Policies and the Editorial Policy Checklist.

Statistics

For all statistical analyses, confirm that the following items are present in the figure legend, table legend, main text, or Methods section.

n/a	Confirmed
☐	☒ The exact sample size (*n*) for each experimental group/condition, given as a discrete number and unit of measurement
☐	☒ A statement on whether measurements were taken from distinct samples or whether the same sample was measured repeatedly
☐	☒ The statistical test(s) used AND whether they are one- or two-sided *Only common tests should be described solely by name; describe more complex techniques in the Methods section.*
☒	☐ A description of all covariates tested
☒	☐ A description of any assumptions or corrections, such as tests of normality and adjustment for multiple comparisons
☒	☐ A full description of the statistical parameters including central tendency (e.g. means) or other basic estimates (e.g. regression coefficient) AND variation (e.g. standard deviation) or associated estimates of uncertainty (e.g. confidence intervals)
☐	☒ For null hypothesis testing, the test statistic (e.g. *F*, *t*, *r*) with confidence intervals, effect sizes, degrees of freedom and *P* value noted *Give P values as exact values whenever suitable.*
☒	☐ For Bayesian analysis, information on the choice of priors and Markov chain Monte Carlo settings
☒	☐ For hierarchical and complex designs, identification of the appropriate level for tests and full reporting of outcomes
☒	☐ Estimates of effect sizes (e.g. Cohen's *d*, Pearson's *r*), indicating how they were calculated

Our web collection on statistics for biologists contains articles on many of the points above.

Software and code

Policy information about availability of computer code

Data collection	Thermo Fisher EPU
Data analysis	CryoSPARC **v4.2**

For manuscripts utilizing custom algorithms or software that are central to the research but not yet described in published literature, software must be made available to editors and reviewers. We strongly encourage code deposition in a community repository (e.g. GitHub). See the Nature Portfolio guidelines for submitting code & software for further information.

Data

Policy information about availability of data

All manuscripts must include a data availability statement. This statement should provide the following information, where applicable:

- Accession codes, unique identifiers, or web links for publicly available datasets
- A description of any restrictions on data availability
- For clinical datasets or third party data, please ensure that the statement adheres to our policy

Models and cryoEM maps were deposited in the Protein Data Bank (PDB) and Electron Microscopy Data Bank (EMDB) under the following accession codes: Haspin position 1 (PDB: 9B2S, EMDB: 44113), Haspin position 2 (PDB: 9B2T, EMDB: 44114), and Haspin local refinement (PDB: 9B2U, EMDB: 44115),

Raw cryoEM movies were deposited in the EMPIAR database under the accession code: EMPIAR-11971.

Research involving human participants, their data, or biological material

Policy information about studies with human participants or human data. See also policy information about sex, gender (identity/presentation), and sexual orientation and race, ethnicity and racism.

Reporting on sex and gender	n/a
Reporting on race, ethnicity, or other socially relevant groupings	n/a
Population characteristics	n/a
Recruitment	n/a
Ethics oversight	n/a

Note that full information on the approval of the study protocol must also be provided in the manuscript.

Field-specific reporting

Please select the one below that is the best fit for your research. If you are not sure, read the appropriate sections before making your selection.

☒ Life sciences ☐ Behavioural & social sciences ☐ Ecological, evolutionary & environmental sciences

For a reference copy of the document with all sections, see nature.com/documents/nr-reporting-summary-flat.pdf

Life sciences study design

All studies must disclose on these points even when the disclosure is negative.

Sample size	For immunofluorescence cell studies N= 3 independent experiments with n ≥ 25 cells/condition. These are typical sample sizes in the field and provided a clear answer with a high statistical significance for these experiments.
Data exclusions	No data was excluded for the analyses
Replication	Cell-based studies were performed with 3 biological replicates
Randomization	For immunofluorescence cell studies, cells in M-phase were randomly chosen.
Blinding	No blinding was performed.

Reporting for specific materials, systems and methods

We require information from authors about some types of materials, experimental systems and methods used in many studies. Here, indicate whether each material, system or method listed is relevant to your study. If you are not sure if a list item applies to your research, read the appropriate section before selecting a response.

Materials & experimental systems

n/a	Involved in the study
☐	☒ Antibodies
☐	☒ Eukaryotic cell lines
☒	☐ Palaeontology and archaeology
☒	☐ Animals and other organisms
☒	☐ Clinical data
☒	☐ Dual use research of concern
☒	☐ Plants

Methods

n/a	Involved in the study
☒	☐ ChIP-seq
☒	☐ Flow cytometry
☒	☐ MRI-based neuroimaging

Antibodies

Antibodies used	anti-H3 (Abcam #ab1791) , anti-H3T3ph (Sigma-Aldrich #04-746), anti-rabbit HRP-conjugated secondary antibody (Invitrogen #31460)
Validation	All antibodies commercially validated. Abcam validation statement for Abcam #ab1791: "Abcam antibodies are extensively validated in a wide range of species and applications". Sigma-Aldrich quality assurance statement for Sigma-Aldrich #04-746: "routinely evaluated by immunoblot on acid extracted proteins from mitotic HeLa cells (Catalog #17-306) treated with colcemid, but not unmodified recombinant histone H3". ThermoScientific statement for Invitrogen #31460: "Product # 31460 has been successfully used in Western blot, IHC, ELISA and IP applications."

Eukaryotic cell lines

Policy information about cell lines and Sex and Gender in Research

Cell line source(s)	HEK293T (Holland lab)
Authentication	not authenticated.
Mycoplasma contamination	not tested
Commonly misidentified lines (See ICLAC register)	*No commonly mis-identified cell lines were used.*

Plants

Seed stocks	n/a
Novel plant genotypes	n/a
Authentication	n/a